Analysis of Diatom Images using Stereology

Hans W. Sendjaja

This report is submitted as partial fulfilment of the requirements for the Honours Programme of the School of Computer Science and Software Engineering, The University of Western Australia, 2004

Abstract

Diatoms are micro organisms that live in the aquatic environment. They provide various indication of marine ecosystem properties such as water temperature, ecosystem population, and nutrient levels. Recent studies of diatoms has led to the development of the videography technique. Videography minimises the interruption of diatoms' structure during the sampling process, which is important, because interruption to diatoms' structure leads to inaccurate analysis. Unfortunately, the videography image contains noise and undesirable effects that cause difficulties in further analysis of the diatoms. In addition, the videography image only provides 2D information, while the diatoms are in 3D.

In this dissertation I presents a new method of analysing diatom images using stereology. The method consists of two stages. In the first stage, the visibility of the diatoms in the image is enhanced by removing the noise and thresholding the image. Then in the second stage, stereological analysis is applied. Stereology is a technique that allows one to estimate 3D geometrical properties of diatoms from the 2D image of a section or projection. To validate the estimation results, I have implemented a synthetic diatom simulator. The simulator is designed to generate a 3D model of synthetic diatoms and its corresponding projection image. Experiments were carried out to estimate geometrical properties of diatoms from the projection image. Then, the estimation results were compared and analysed with respect to the corresponding actual geometries from the 3D model.

Keywords: Analysis of diatom using stereology, stereology of diatom, analysis of diatom, estimation of diatom properties.
CR Categories: G.1.2 [Approximation] - Approximation of surfaces and contours, G.3 [Probability and Statistics] - Stochastic processes, I.6.6 [Simulation Output Analysis], J.3 [Life and Medical Sciences] - Biology and genetics.

Acknowledgements

Honours year is the time where I have learned many aspects of life. It has been a great pleasure to acknowledge these people that have been helping me along the way. I would be forever indebted to these people.

First of all I would like to thank Dr Peter Kovesi who always looking out for his students and constantly gave me invaluable feedbacks and encouragement. Thanks also to Dr Anya Waite and Prof. Adrian Baddeley for their inputs and additional thoughts.

I would also like to thank Jesus Christ for His blessings. I am grateful to Winnie who has been wonderfully caring and understanding throughout my honours year. Finally, a special thank you to all the honours student 2003 and 2004 for your friendship and constant encouragement. I will never forget the endless moments of laughter, frustration and happiness I shared with you all.

For the readers, I would like to thank you for spending your invaluable time.

‘’So I say to you: Ask and it will be given to you; seek and you will find; knock and the door will be opened” Luke 11:9

Contents

List of Tables

List of Figures

CHAPTER 1

Introduction

Diatoms are unicellular microscopic algae that are approximately 2-500μm in size and exist in aquatic environment. They have an external shell, which is mainly made up from silica and siliceous material. Diatoms form a large deposits of white chalky material, which can be used in cleansers, paints, filtering agents and abrasives [6]. Furthermore, diatoms are an important indicator of our ecosystem health. Depending on species, they can be an indicator of marine ecosystem population, water temperature, water depth, nutrient levels or salinity. Therefore several approaches of analysing diatoms have been developed, ranging from diatom shape analysis to measurements of their aggregations. Unfortunately, laboratory studies of diatoms have suffered from inaccuracy due to the sampling method, which tends to disrupt the natural structure of diatoms [7]. Waite et al. [7] developed a videography technique that captures images of diatoms in the water. However these images are prone to noise. For example, the effect of camera focus makes it difficult to distinguish between diatoms and non-diatoms (see Figure 1.1). Therefore, a series of image pre-processing technique must be applied to denoise the image. Also the images only provide a 2D projection of the 3D diatoms.

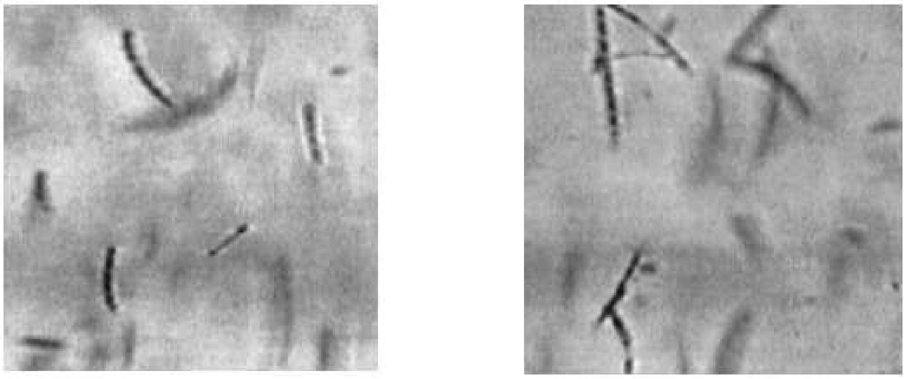

Figure 1.1: Diatom images.

To my knowledge, analysing diatom using stereology has never been done by anyone. There are various definitions of stereology, however Baddeley [8] describes it the best, which says, "Stereology originated as the problem of studying a three-dimensional physical object from random two-dimensional plane sections or projections, and in particular of estimating geometrical parameters such as volume, surface area, length and total curvature". The International Society of Stereology was founded in 1961. Its members came from different fields including mathematics, statistics, biology and materials science. Stereology was widely applied to different disciplines such as anatomy, material science and plant and soil study [9, 10, 11]. The importance of stereology in analysing diatoms is to yield several geometrical properties of diatoms (e.g. size, length, area, volume, volume density, number density) using a limited two dimensional image. The geometrical properties of diatoms are useful for scientists in studying the behaviour of diatoms.

I propose a new method for analysing diatom without disturbing the structure of diatom. The method consists of two stages, which are the image pre-processing and the stereology. The diatom images are supplied by The Centre For Water Research UWA. They obtained the images through the videography technique described by Waite et al. [7]. These images are in the RGB format. These images need to be pre-processed to reduce noise. Once pre-processed, the output images will be in binary format that contain white objects (diatom) on a black background. In the second stage, I will demonstrate the use of stereology to estimate diatom geometrical properties based on the binary image. However these properties will not be reliable without verifying them with actual diatom's properties. Unfortunately, it is difficult to obtain a physical measurement of diatom properties, especially without breaking their geometrical structures. Therefore, I created a simulation of diatoms that aims to model the actual diatom and hence, allows us to obtain physical measurement of diatoms geometries. The simulation will produce three outputs, that are as follows:

- 3D model of diatom that can be rotated in any orientation.
- Projection image of the 3D model of diatoms, which is taken from a random viewpoint.
- List of diatom actual geometrical properties derived from 3D model, such as length, surface area, and volume. These properties are then compared with properties derived from the projection image.

1.1 Overview

This dissertation is organised into six chapters. Chapter 2 reviews some of the work that has been done by other researchers in analysing diatoms, including the videography technique used in this project to obtain diatom images. Chapter 3 describes the pre-processing stage of diatom images. Following that, Chapter 4 describes how stereology is applied to the processed diatom images. In applying stereology, most work has been done getting 3D information from 2D section. Here we have to work with 2D projection. This is harder and there are fewer stereological results for 2D projection data. Both Chapters 3 and 4 are structured in the same way in that each chapter contains a literature review, methodology, and an experimental result section. Chapter 5 presents simulation results of diatom geometrical properties derived from synthetic models and from their 2D projections. Finally, Chapter 6 gives a summary of this dissertation as well as further study that can be made to this project.

CHAPTER 2

Diatom Analysis

Diatoms have been analysed in a variety of ways. Depending on the objective of the research, scientists have to carry out certain procedure to sample diatoms. Since diatoms are fragile micro organisms, it is inevitable that sampling diatoms on the microscope plate will disturb their natural structure, especially if a technique such as electronic particle counting was to be introduced to the sample [7]. Therefore a technique of sampling diatom without disturbing their structure is desirable if one wants to achieve a fine degree of accuracy. In this chapter I will describe a technique of sampling diatom images via videography as well as other researches that have been done in the area of diatom analysis, particularly on aggregation measurement and diatom shape analysis.

2.1 Measuring Diatom Aggregation using Videography

Waite et al. [7] proposed a new method for analysing diatoms aggregation. Aggregation of diatoms affects the sedimentation rate of the intense pulses of carbon formed during diatom blooms. The study of aggregation dynamics have been troubled by the unavoidable disruption of aggregates in laboratory flocculators due to subsampling and electronic particle counting. This aggregate disruption prevents an accurate measurement of aggregation rate and makes observation of particle structure impossible. The authors use the combination of a high-resolution video recording and an image analysis application to analyse the aggregation of Chaetoceros neogracile 6 to 8 μm. The water sample that contains cells of Chaetoceros neogracile was placed inside a Couette chamber of a rotating flocculator. When the chamber is rotated, a known laminar shear was generated, that causes cells to collide and form aggregates depending on stickiness of cells. To examine the aggregation, they set up a high resolution imaging system and video recorder. The focus was directed to the zone of laminar shear within the chamber. The imaging system produced a high-contrast bright field exposures at 60 images per second, which then recorded by a Sony video recorder. Once the images have been obtained, the next step is to carry out an image processing activity. The image processor selected one image in every 60 images for analysis. Individual cells in the image were isolated using a thresholding and an edge detection technique. The cross sectional area of each cell was then calculated and used as a measurement of a diatom aggregation. In addition to cross sectional area, they also made an assumption about nearest neighbour distance that states that aggregations of Chaetoceros neogracile cells were not more than 30 μm apart. To determine whether cells formed a single aggregate, they developed a method by expanding a bounding circle called halo 30 μm from the centre of each cell, through a series of erosions and dilations operation. After that, depending on the contiguousness of the halo, they determine whether the individual cells formed a single aggregate. Finally, they shrank back the halo to obtain a single measurement of aggregate size and volume. The mean size data was calculated from a group of 50 consecutive images in 0.32 μm of culture medium sampled over the 50 seconds of the experiment.

Once the image processing is done and the required data have been collected, they carried out Kiorboe's [12] stickiness calculation to measure stickiness of cells. The stickiness of cells depends on the increase in mean particle over time as it collides and adheres to each other to form aggregates, whether it is a doublet (2 cells) or a triplets (3 cells), within the flocculator. The measurement is important because increases in stickiness of culture have significant implications for the dynamics of diatom blooms [7].

To obtain results and observations, Waite et al. [7] conducted an experiment with 12 litres batch cultures of Chaetoceros neogracile. The duration of the experiment was 12 days and every second day, 1 litre of each culture was taken for stickiness measurement, placed in the Couette chamber for 2 hours. The video recorder then records the first 45 minutes of each experiment continously. They also made a comparative measurement using Elzone Particle Counter to measure the culture size distribution. By comparing the stickiness value, it appears that the videography technique was superior in sampling frequency and consistency of data. Additionally, with videography, we can actually resolve the singlets and doublets that we are interested in, without the need of averaging over a large aggregate volume. Finally, the videographic measurement also records extra information, which is useful for studying particle dynamics, including an individual cell morphology, an aggregate structure and its porosity, and the movement of particles within an imposed shear.

2.2 Diatom Shape Analysis

Another approach for analysing diatoms is by their shape [13, 14, 15]. This approach is concerned with the classification of diatom shapes rather than the measurement of aggregation. The diatom classification process mainly involves diatoms' contour information.

Vargas et al. [13] proposed three stages in the process of diatom classification from debris: segmentation, feature extraction and classification of the main diatom classes found. Firstly, the segmentation stage consists of two parts that are an image acquisition at low resolution and a further analysis at higher magnification. Different diatom images were sampled from fresh water by means of optical peripheral. The images were then digitised into 8 bit/pixel and 256 x 256 pixel format. Once digitised, the images are still at low resolution and it is difficult to discriminate diatoms from non-diatom objects. The difficulty is due to the similarity of grey level intensities between diatoms and the background. Therefore, Vargas et al. tested several thresholding methods and found that the Otsu [16] threshold method give the best result. Although the Otsu method remove a substantial number of debris particle that are not required to be analysed, the authors still argue that it is difficult to elucidate which parts of the image are debris and which parts deserve to be analysed. Following the image pre processing that omits segmented diatom images, the next step in the first stage of diatom classification is to track diatom contours. Vargas et al. proposed a new method for tracking a diatom's contour based on eight connectivity and neighbourhood of the contours. The new method scans the image from top left corner until a new region pixel (P_0) is found. As there are no more pixels above P_0 belonging to the region, the initial direction is taken in order to look for a new pixel and assigned to zero. The search ends when the two first pixels are found again. The outcome of this method allows one to obtain closed contours even when the shape is noisy and irregular. The second stage of diatom classification process is feature extraction. Vargas et al. evaluated a number of features/descriptors, which include perimeter, area, convex area, measure of compactness, major and minor axis length, eccentricity, solidity, the seven Hu moments [17] and the first ten normalised Fourier descriptors [17]. Based on these features, in the last stage the authors classified diatoms into the four selected types of diatom shapes; circular, elliptical, elongated and squared. The classification was made using a nearest neighbor algorithm applying the Mahalanobis distance [13]. A similar approach was taken by Shahbazkia et al. [15] that classifies classifies diatoms based on the contour information. They use several shape descriptors described in the following to characterised diatom outlines.

Symmetry: In order to compute symmetry, Shahbazkia et al. [15] uses the correlation between the two half contours obtained by folding the part of a contour lying on one side of an assumed axis onto the other side. They defined a symmetry as the difference between the two half-curves as half of the area that they enclose.

Convexity by area ratio and perimeter ratio: The convexity of diatom is measured by either the ratio of the areas or the perimeters of the convex hull and the original contour.

Circularity: Circularity of a diatom can be measured by the eccentricity formula

$$e = (m_{20} - m_{02})^2 + m_{11}^2/(m_{20} + m_{02})^2 \tag{2.1}$$

where m_{ij} is the ij central moment of the outline.

Ellipticity: Ellipticity of a diatom can be measured by the following formula

$$\frac{\sqrt{(m_{20} + m_{02}) + \sqrt{(m_{20} + m_{02})^2 + 4m_{11}^2}}}{(m_{20} + m_{02} - \sqrt{(m_{20} - m_{02})^2 + 4m_{11}^2}} \tag{2.2}$$

where m_{ij} is the ij central moment of the outline.

Rectangularity: Rectangularity of diatom is measured by the following formula

$$rec = \frac{area\ of\ the\ outline}{(length \times width)} \tag{2.3}$$

Elongatedness: Elongatedness of a diatom is measured by the following formula

$$E = \frac{area}{max\ thickness\ of\ minimum\ bounding\ box} \tag{2.4}$$

Size ratio: Size ratio of a diatom is measured by the following formula

$$R = \frac{width}{length} \tag{2.5}$$

Compactness: Compactness of a diatom is measured by the following formula

$$C = \frac{area}{perimeter^2} \tag{2.6}$$

Unlike Vargas et al. [13], Shahbazkia et al. [15] used the Kohonen mapping to distinguish diatoms by their shape. Despite their different approach in mapping technique, Vargas et al. and Shahbazkia et al. achieved a similar result in the classification of diatom shape.

Note that all studies of diatom discussed above only present information in 2D projection space (e.g. projections of size, length, area) and do not present any information in 3D space (e.g. surface area, volume, volume density, number density).

CHAPTER 3

Diatom Image Enhancement

Images of diatom obtained by a videography technique contain a significant amount of noise that obscures the diatoms (see Figure 3.1).

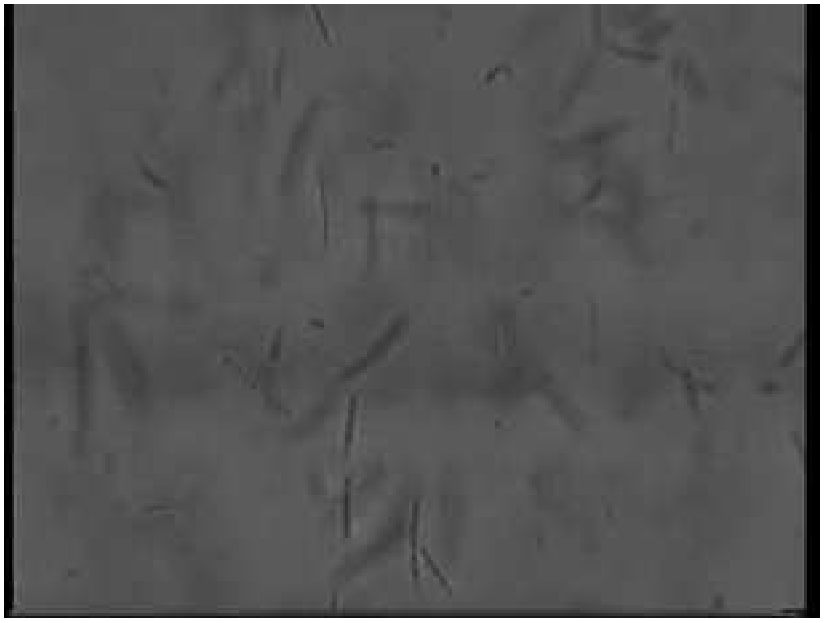

Figure 3.1: The videography image of diatoms.

Thus, it is compulsory to pre-process these images before analysing them. In the first stage of analysing diatoms using stereology, images of the diatoms are pre-processed to reduce noise and enhance the visibility of the diatoms. The main techniques involved in the diatom image enhancement are:

- Image Conversion.
- Image Filtering.
- Image Denoising.

- Image Thresholding.
- Morphological Operations.

Diatom images are pre-processed by applying each technique above in orderly fashion. First, the diatom image is converted to a grey scale format (depending on the initial format of the image, this step may not be necessary), then, a high pass filter was applied to remove out of focus diatoms from the image. Unfortunately this increases noise in the image. Noise reduction using the phase preserving denoising algorithm was applied to clean up the noise. Finally, the image was thresholded and morphological operations were applied to reconstruct the image of diatom in a binary representation.

In this chapter, I will describe the methodology and the implementation of a diatom image processing algorithm. Firstly, I will review existing image enhancement techniques that are relevant to diatom image enhancement. This will be followed by results of the experiments involving each step of the diatom image enhancement.

3.1 Methodology

3.1.1 Image Conversion

An image can be in many formats, such as ALIAS, BMP, GREY and RGB. It may necessary to convert an image from one format to another due to requirement of certain type of algorithm. One conversion that is important in processing the image of diatoms is the conversion of an RGB image to a grey scale image format. This conversion is achieved by eliminating the hue and the saturation while maintaining the luminance. Such image conversion algorithm has now become a standard function of most image processing tools.

3.1.2 Image Filtering

Diatom Images will contain views of out of focus diatoms. In processing a diatom image, our objective is to enhance diatoms that have been blurred due to the effect of camera focus such that, the interpretation of in-focus diatoms has been troubled by the presence of the out of focus diatoms. Therefore we need to remove these out of focus diatoms, leaving only the diatoms that are in focus.

In the frequency domain, the in-focus diatoms are correspond to the high frequency components of the image, while the out of focus diatoms correspond to the low frequency components of the image. Since we want to keep the in-focus diatoms and remove the out of focus ones, a high pass filter is applied to the diatoms image. The high pass filter filters only the high frequency components of the image that means only the in-focus diatoms get filtered in.

3.1.3 Image Denoising

Other than removing the out of focus diatoms, high pass filter also amplifies the noise in the image. The aim of image denoising is to remove the noise.

Denoising of images is typically done by transforming image into some domain where the noise component is more easily identified. Kovesi [2] proposed a phase preserving denoising of images, based on the decomposition of a signal using complex-valued wavelets. The main goal of the this work is to overcome several issues with previously implemented wavelet based denoising, which are wavelets selection, threshold setting and features in an image affected by the thresholding operation. The issue in selecting wavelets arose because neither orthogonal nor bi-orthogonal wavelet has been identified as being the best for denoising. The author addressed the issue of wavelets selection by selecting log Gabor wavelets. The selection was because these wavelets have the desirable linear phase or near linear phase response. The wavelet shrinkage threshold is the most crucial parameter in the denoising process. The author has implemented an automatic determination of shrinkage threshold from the statistics of the amplitude response of the smallest scale filter pair over the whole image. The author has also proved that this approach is very successful.

According Oppenheim and Lim [18], one quantity that appears to be very important in human perception of images is phase. Based on the previous statement, the quality of feature in an image perceived by human is related to the phase information of an image. Thus preserving phase information of an image is an important constraint in denoising images. Figure 3.2 shows the comparison between the result of applying phase preserving denoising algorithm to a grey scale image and the result obtained by applying standard discrete wavelet denoising scheme (the MATLAB `wdencmp` function using the 'symlet8wavelet').

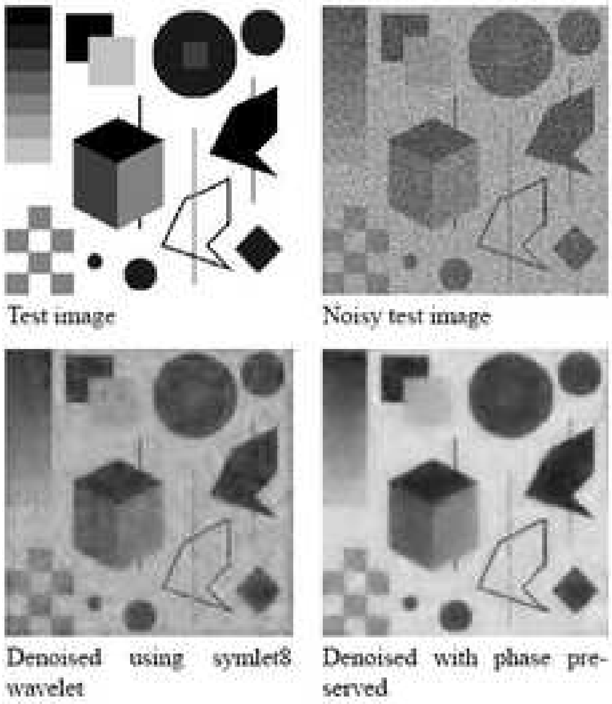

Figure 3.2: The results of phase preserving denoising algorithm [2].

The denoised image with phase preserved is perceptually better than the one denoised using the standard discrete wavelet.

3.1.4 Image Thresholding

For diatom image analysis, a binary representation of an image is a desirable. Specifically, the binary image should contain white objects (diatoms) on black background. A binary image is typically obtained by thresholding a grey scale image. This is achieved by setting pixels above the threshold to 1 (white), and the rest to 0 (black). However, choosing a threshold value can be difficult, especially if the grey levels of the object and the background are fairly close. Canny [19] suggested hysteresis thresholding for such case. In hysteresis thresholding, two threshold values are selected. All pixels with values above the first threshold are marked as part of a diatom, whilst all pixels that are adjacent to points that have been marked as part of a diatom and with values above the second threshold are also marked as part of a diatom.

Nevertheless, there are no thresholding algorithms that perfectly segregate objects from a background. The thresholded image may contain 'salt and pepper' noise due to the difficulty in differentiating between foreground and background in a grey scale image. In addition, parts of feature in an image may be incomplete. Therefore, cleaning and reconstructing the image is compulsory.

3.1.5 Morphological Operations

One way to reconstruct objects in the binary image is using mathematical morphology. Morphological operations are based on two sets of transformations by a structuring element. They are erosion (shrinking the object) and dilation (expanding the object). The structuring element can be in any shape, but circle is the most commonly used shape. Erosion and dilation are useful for reconstructing objects in the binary image. However, they will not give any benefit unless both of them are combined. Two types of combinations are:

1. Opening that is an erosion followed a dilation.
2. Closing that is a dilation followed by an erosion.

Opening helps to clean 'salt and pepper' noise, while closing, is used to restore parts of the object that has been missing.

3.2 Implementation

3.2.1 Implementation Environment

All techniques described previously were implemented using MATLAB version 6.5 on Red Hat Linux operating system. The experiment was carried out on Pentium 4 CPU 2.8 GHz with 496 MB of RAM. A collection of diatom images were supplied by The Centre for Water Research UWA and one image was selected for input. The aim of this experiment is to illustrate results of each step in the diatom image enhancement process.

3.2.2 Diatom Image Conversion

Most images of diatom obtained were in the RGB format. Therefore, the implementation of processing a diatom image was initiated by converting the image into the grey scale format. Otherwise, if the images are already in the grey scale format, conversion is not necessary. First, the original image was converted using MATLAB function `rgb2gray` to obtain a grey scale version of original image. Then the grey scale image is trimmed on all sides to eliminate edges effects (see Figure 3.3).

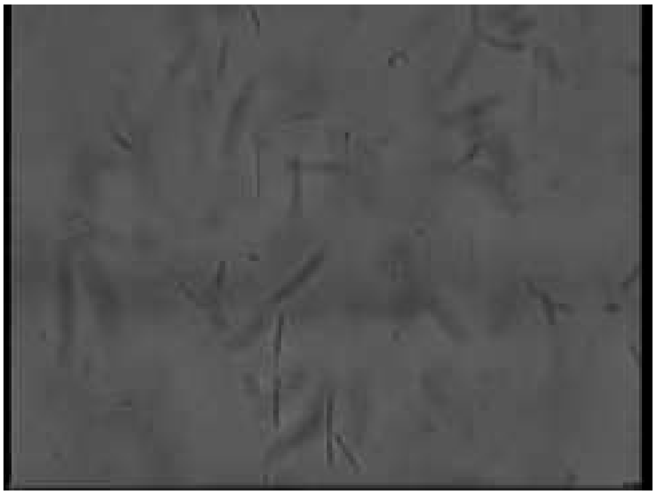

(a) Original image.

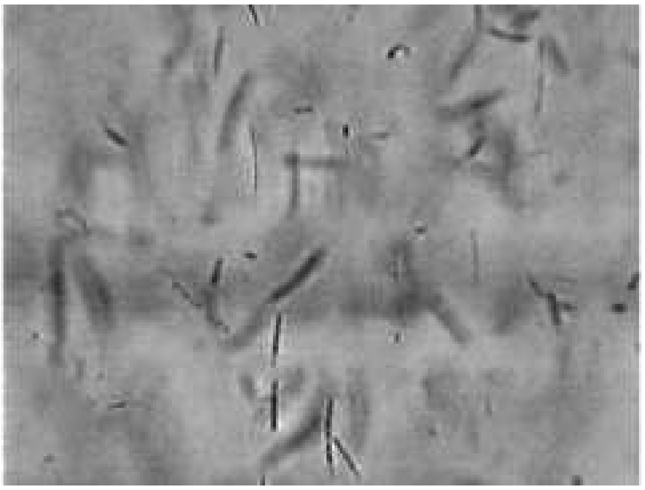

(b) Grey scale image.

Figure 3.3: The result of converting an RGB diatom image of size 256×256 pixels to grey scale image.

3.2.3 Diatom Image Filtering

As shown in Figure 3.3(b), the diatom image is blurred by the camera focus effect. This image contains diatoms that are in focus and diatoms that are out of focus (blur objects). Therefore, a convolution of the image using high pass filter in the frequency domain was applied to filter the in-focus diatoms. Firstly, assuming that the image is in a grey scale format, a two-dimensional Fourier transform matrix of the image is constructed via MATLAB function `fft2` (see Figure 3.4(b)). In addition, a high pass filter with the same size as the image is generated via the `highpassfilter` function (see Figure 3.4(c)). Finally, I convolved the Fourier transform of an image with the high pass filter to remove the camera focus effect (see Figure 3.4(d)).

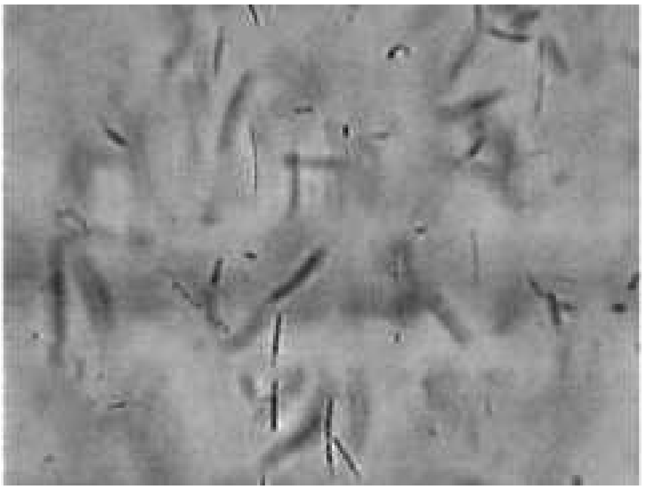

(a) Original image.

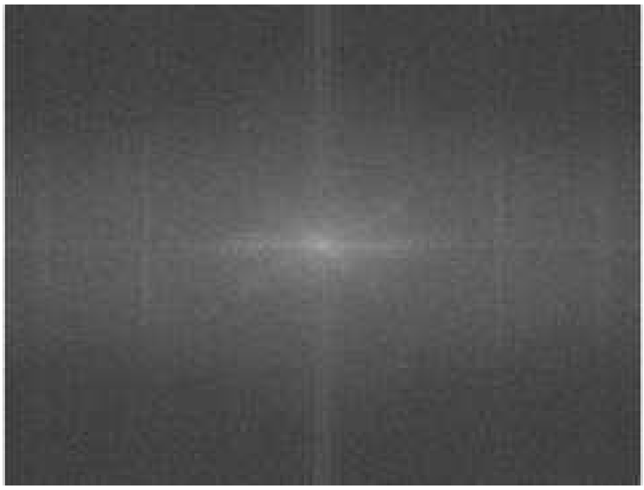

(b) Fourier Transform of the original image.

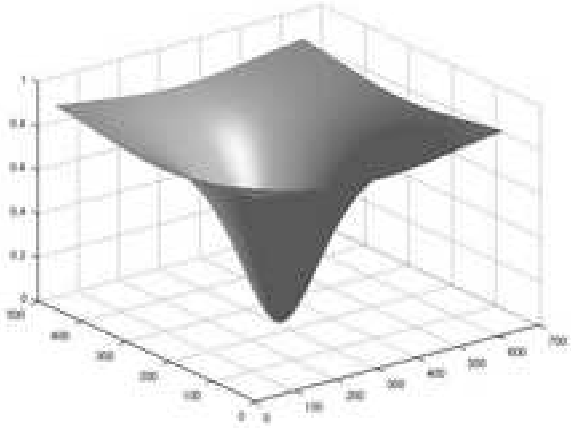

(c) 3D surface plot of the High Pass Filter.

(d) Filtered Image.

Figure 3.4: The results of convolution in frequency domain using a high pass filter.

3.2.4 Diatom Image Denoising

Figure 3.4(d) shows a significant amount of noise still present after the filtration step. Therefore, a phase preserving denoising algorithm was applied in order to reduce the amount of noise. This algorithm was selected because it has been proved to generate a perceptually better image than the one generated using standard algorithm [2]. The algorithm managed to reduce a considerable amount of noise while preserving the phase information. The results of the denoising process is shown in Figure 3.5.

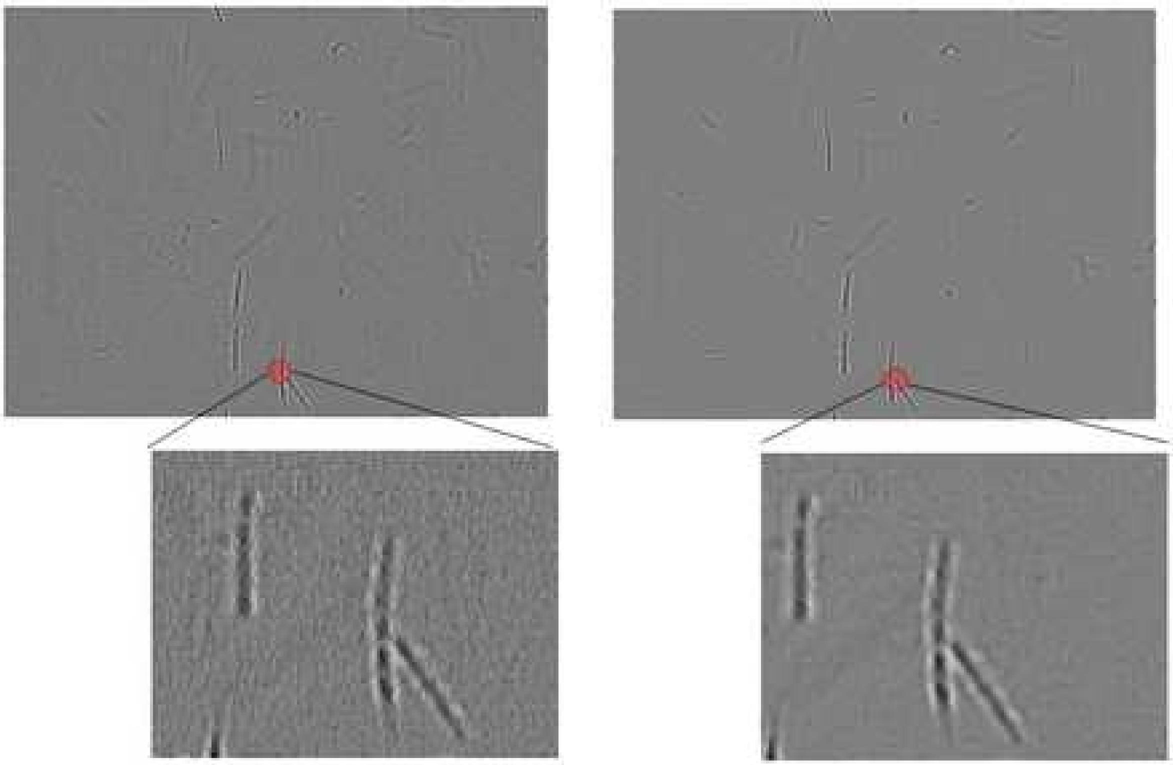

(a) Before denoising process.

(b) After Denoising process.

Figure 3.5: The result of phase preserving denoising the diatom image.

3.2.5 Diatom Image Thresholding

Figure 3.5(b) shows that the denoised image of diatom has a close grey level between its foreground and background. Thresholding with a single threshold value will not give the best result. Therefore, the hysterisis thresholding algorithm was applied to threshold the image. However the perception quality of the binary image is highly dependent to the two threshold values used. For a $256x256$ image, I used an upper threshold value of 2 and a lower threshold of 0.5. Figure 3.6

shows that hysterisis thresholding gives more useful result than the single value thresholding.

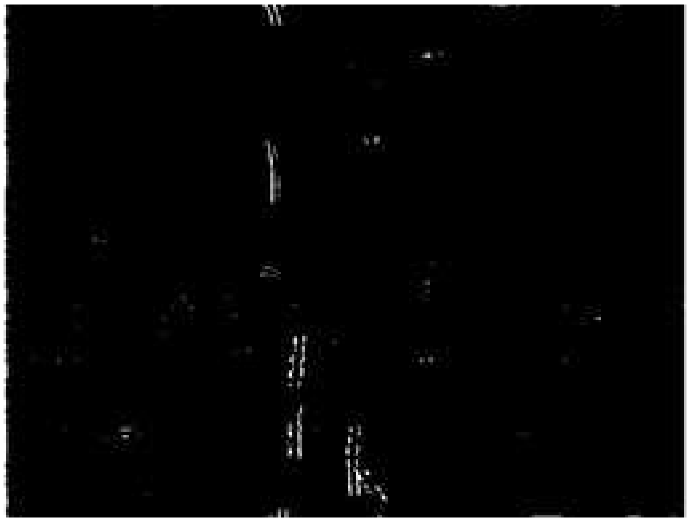

(a) Single value thresholding with threshold value of 2.

(b) Hysterisis thresholding with upper threshold value of 2 and lower threshold value of 0.5.

Figure 3.6: Comparison of results between single value thresholding and hysterisis thresholding.

3.2.6 Morphological Operations

The final step in the diatom image enhancement is to reconstruct the binary image in order to achieve a better perception quality. This step involves eliminating the presence of 'salt and pepper' noise and to restore parts of the feature that have been lost due to the thresholding operation. A set of morphological operation was applied to the binary image. Firstly, an opening was applied to eliminate the remaining 'salt and pepper' noise. Following that, a closing operation was applied to restore the shape of the feature. All morphological operations were implemented using MATLAB function `imopen` and `imclose` with a circular structuring element. Figure 3.7 shows the result of applying morphological operations to Figure 3.6(b).

Figure 3.7: The result of applying morphological operations.

Figure 3.7 shows a much better image for analysing the diatoms compare to the original grey scale image in Figure 3.1. Diatoms are clearly shown as white features on a black background. Hence, further analysis of diatom will be performed focusing on the white feature of the binary image. To my knowledge, there is no appropriate metric of measurement that assesses the fidelity of the binary image. However, the phase information of the image has been preserved during the denoising process.

CHAPTER 4

Application of Stereology on a Diatom Image

The second stage of analysing diatom images is using stereology to deduce geometrical properties of diatoms. Stereology is a technique which attempts to explore three dimensional spaces, when only two dimensional sections through solid bodies or their projections on a surface are available [1]. Stereology works on either the two dimensional section image of a solid body or its projection image. To the extent of my knowledge, the majority of stereology has been applied in two dimensional images of a section rather than its projection. Unfortunately, images of diatoms are mainly the result of projection. It is impossible to obtain the image of a diatom's section, because they are microstructures and very fragile.

In this chapter, I will present methods of stereology and their implementation on a diatom image. First, I will review existing stereology methods on section image and projection image. Then, I will describe the implementation of stereological methods using the diatoms image as an input.

4.1 Section

Stereologists often deal with two dimensional (2D) forms of an object to avoid complications in three dimensions (3D) [3]. One way to get a 2D form is through sectioning the object. A section is an infinitely thin plane that is part of a solid body and obtained by slicing through the cross section of the body. By obtaining the section of the object, stereologists can estimate some useful geometrical properties. The following subsection describes several geometrical properties which can be obtained from the sections of an object.

4.1.1 Total Volume

Howard and Reed [3] demonstrated how one can estimate a volume of an object using the Cavalieri method, when only images of its section are available. Suppose we are interested in the volume of an arbitrary shaped object, we can create a series of section with a known thickness by slicing the object in parallel with serial sections as shown in Figure 4.1. The number of sections hitting the object in the illustration is seven, which gives rise to eight slabs of the object. The second slab is extracted from the object and it can be viewed as a 2D image containing a cross sectional area of the object shaded in light grey.

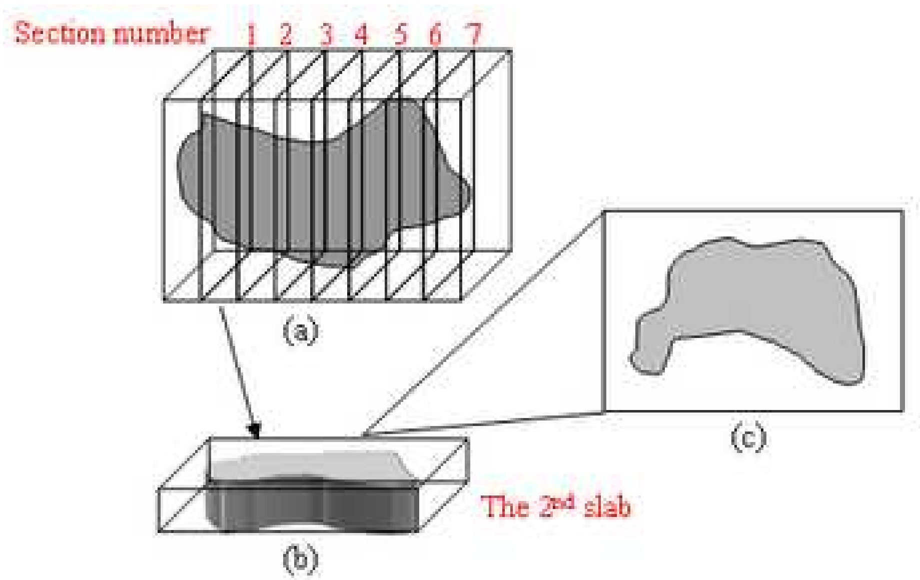

Figure 4.1: (a) A 3D object. (b) A section of the 3D object. (c) A 2D view of the object's cross sectional area [3].

Once we have obtained a series of section images, the volume of the object can be estimated by summing the areas and multiplying by it the slice thickness T.

$$\hat{V} = (T \times A_1) + (T \times A_2) + ... + (T \times A_n) = T \times \sum A_i \tag{4.1}$$

where $\hat{V}$ = estimated volume of the object.
T = slice thickness.
A = cross sectional area as shown in Figure 4.1 (c).

Assuming that the image in Figure 4.1 (c) is a binary image, the cross sectional area can simply be measured by calculating the number of pixels which fall into the region of interest. There have been several implementations of the Cavalieri method including estimation of human body volume and animal brain volume [20, 21].

4.1.2 Volume Fraction

Aside from the total volume, stereology by section can be used to estimate a component volume and a volume fraction. Estimation of volume fraction was first proposed by Delesse in 1847 [3]. He stated that "the area of the phase per unit area of the section was an excellent predictor of the volume of that phase per unit volume of the crushed rocks". Hence his statement can be expressed by:

$$V_V(Y, ref) = A_A(Y, ref) = A_Y/A_{ref} \tag{4.2}$$

where $V_V(Y, ref)$ = volume of Y per unit volume of reference space.
$A_A(Y, ref)$ = area of Y per unit area of reference space.

Figure 4.2 illustrates a section where the phase of interest Y is represented by the dark grey features and the reference area is represented by surrounding light grey region.

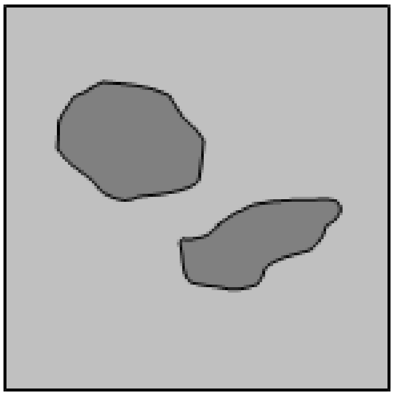

Figure 4.2: A section of an object that contains single phase[3].

Delesse idea was then modified in 1898 by Rosiwal. Instead of using area, Rosiwal uses a series of random lines superimposed on the section [3]. Then, the volume fraction of the phase of interest can be expressed as the length of line intersects the phase of interest per total length of line used. Rosiwal's statement is formulised by:

$$V_V(Y, ref) = L_L(Y, ref) = L_Y/L_{ref} \tag{4.3}$$

where $V_V(Y, ref)$ = volume of Y per unit volume of reference space.
$L_L(Y, ref)$ = length of line intersects Y per total length of test line superimposed on the section.

In 1930, Thompson further modified the method by using randomly positioned point grid [22]. He showed that the volume fraction of the phase of interest can be estimated by superimposing grid of points. Hence the number of points fall in the phase of interest per total number of points falling into the whole section is an unbiased estimator of volume fraction.

$$V_V(Y, ref) = P_P(Y, ref) = P_Y/P_{ref} \tag{4.4}$$

where $V_V(Y, ref)$ = volume of Y per unit volume of reference space.
$P_P(Y, ref)$ = number of points falling into region of Y per total number of points falling into the whole section.

In fact, Thompson used point counting to estimate areas. Based on Equations (4.2),(4.3),and (4.4) we can derive:

$$V_V = A_A = L_L = P_P \tag{4.5}$$

which means that the volume fraction of an object can be estimated by its area fraction, length fraction, or point fraction.

Figure 4.2 illustrates a single phase material, where there is only one type of phase of interest and the whole section as the reference space. In the case of multi phase material, volume fraction can be estimated in the same manner as in the single phase case. Figure 4.3 shows an example of multi phase case where we want to estimate the volume fraction of nucleus per unit volume of nerve cell body. In this case, the reference space is the nerve cell body, rather than the whole section.

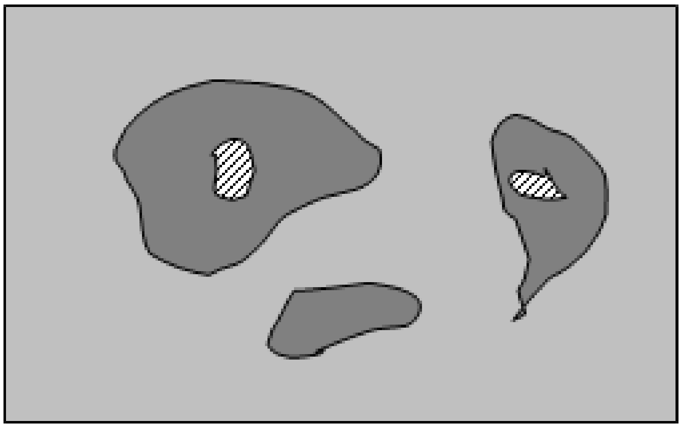

Figure 4.3: An example of multiphase material. The areas that shaded by diagonal lines are the phase of interest (nucleus), the dark grey area is the reference space (nerve cell body), and the whole section is indicated by light grey region [3].

There have been several implementation of estimating volume fraction including the estimation of the volume density of nuclei in invasive ductal breast carcinomas by Villalobos and Perula [23] and the estimation of fibrin type fibrinoid in human placenta by Mayhew [24]. Both Villalobos and Mayhew used a point counting (point fraction) method to estimates the volume density of the phase of interest.

4.1.3 Number Estimation

Another important geometrical properties that stereology can offer is an estimation of the number of particles that are within a well defined reference space. Although counting the number of particles in a tissue section seem to be straight forward and easy, there are several techniques in stereology that have been developed for this task. A popular counting technique in stereology is the 'disector' technique [25]. The technique assumes we have two consecutive images of section, one is the reference section and the other is the lookup section. Before we proceed further, it is important to know that a particle transect is a 2D profile of a sectioned particle. If a particle transect seen in the reference section cannot be found in the look up section, then it is counted. Gundersen [4] proposed an unbiased counting frame which is used to determine whether a particle transect deemed to be seen or not. Figure 4.4 illustrates a 2D field of view containing several 2D particles transect superimposed by Gundersen's unbiased counting frame. The counting frame consists of a solid forbidden line, which extends above and below the field of view to infinity, and a dashed acceptance line. Any transect that is cut by the forbidden line is not counted (i. e. a and b). Transects that are falling fully inside the frame (i.e. c), or those that are cut by the acceptance line and do not cut the forbidden line (i.e. d and g), are counted.

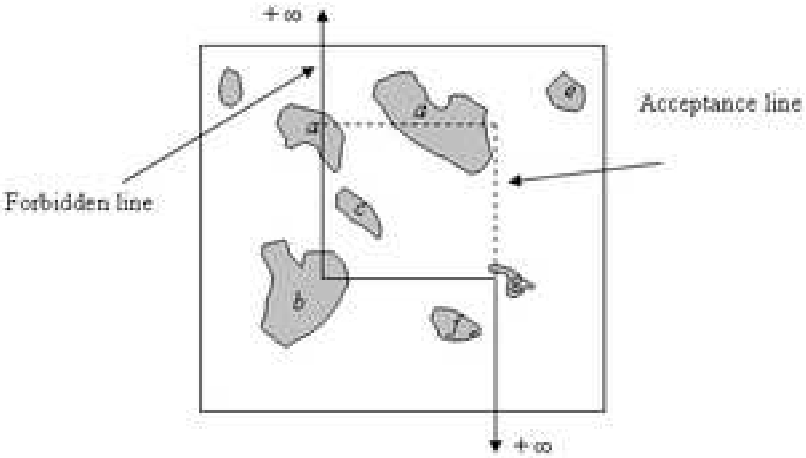

Figure 4.4: Gundersen counting frame [4].

The application of Gundersen's counting frame in dissector technique is illustrated in Figure 4.5. A 3D object has been sectioned into eight sections with a known thickness. The dissector regards sequential sections such as section 1 and 2, as a reference section and a look up section respectively. For each transect correctly sampled in the reference section (i.e. a, b and c) a corresponding transect is sought in the look up section. If no corresponding transect is found anywhere in the look up (in this illustration, transect a is missing, indicated by the star) this particle is counted in 3D space.Note that although transect from particle b that is seen in the look up section is outside the dashed line, this particle is not counted in 3D because it is still present in the look up section. Particle c is not counted in 3D because its transect is still seen in the look up section. Therefore only one particle (i.e. a) is counted.

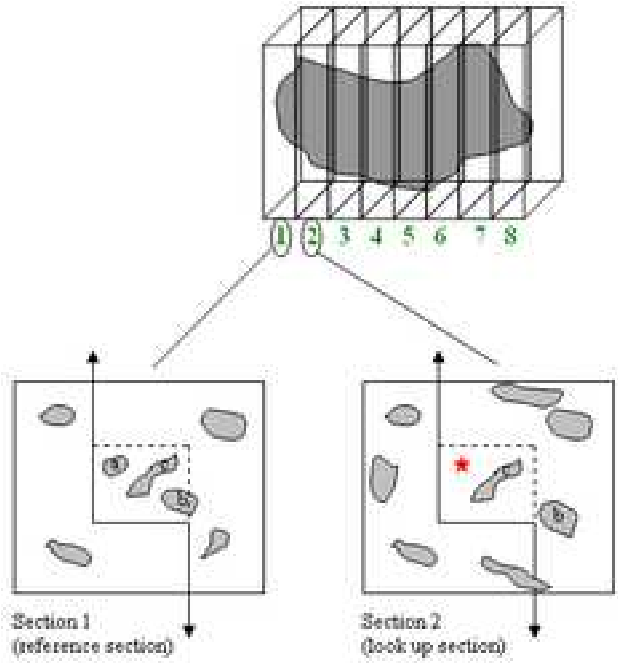

Figure 4.5: Disector counting technique [3].

The disector technique is performed through all sections sequentially and a cumulative count of particles is recorded. The numerical density is estimated using the following formula :

$$N_V = \frac{1}{a \cdot h} \cdot \frac{\sum Q}{\sum P} \tag{4.6}$$

where N_V = numerical density.
a = area of the counting frame.
h = disector height.
$\sum Q$ = sum of particles counted.
$\sum P$ = sum of frames associated with points hitting the reference space.

Tomori et al. [26] have developed a disector program which is based on the disector counting technique described above. They have successfully estimated the number and numerical density of mesophyll cells in a Norway spruce needle. The process took 2-4 minutes for one stack of sections and less than 100 minutes for one needle.

4.1.4 Length Estimation

Howard and Reed [3] showed that a 2D probe such as plane can be used to measure the length of a feature and its length density. Figure 4.6 illustrates the estimation of the linear feature length from its intersection with the plane. In Figure 4.6 (a), a random plane intersects a simple linear feature once, whereas in Figure 4.6 (b), a more convoluted linear feature is intersected by a random plane three times. The Figure shows that the number of intersections per unit area on plane (b) is higher than on plane (a), which is related to the length of linear feature.

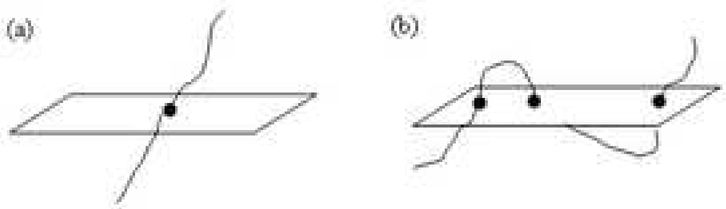

Figure 4.6: (a) Intersection of linear feature with a plane. (b) Intersection of convoluted feature with a plane.

An important requirement to estimate a feature length using a 2D plane is the plane orientation. An unbiased estimation of length requires the orientation of the plane to be isotropic [1]. If we have an anisotropy plane, such as shown in Figure 4.7, our estimation of length would be biased according to the plane orientation. The resulting density of intersections per unit area of plane is seen to be highly dependent upon the orientation of the plane with respect to the features.

In practice, it is often hard to determine the orientation distribution of the linear features. In order to ensure that the number of intersections per unit area is an unbiased estimator of length density, we therefore require the planar probes themselves to be isotropic. The length density of features in volume is estimated from the following formula:

$$L_V(Y, ref) = 2 \cdot \frac{\sum_{i=1}^{n} Q_i}{a \cdot \sum_{i=1}^{n} P_i} \tag{4.7}$$

where L_V = length of Y per unit volume of reference space.
Q = number of profiles sampled by the frame.

[1] Identical in all direction or invariant with respect to direction

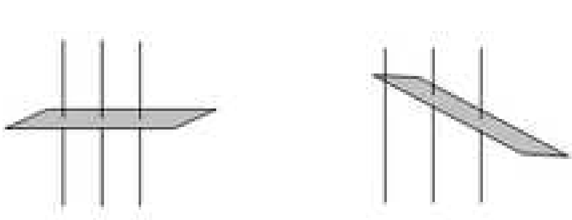

(a) (b) (c)

Figure 4.7: A series of perfectly anisotropy linear features intersects a series of planes which are respectively (a) normal, (b) oblique, (c) parallel to the axis of the anisotropy [3]

a = area of the counting frame.
P = number of frames used.

The number of profiles sampled by the frame (Q) is estimated by using Gundersen's counting frame as in disector technique.

Length Estimation using Vertical Section

Another approach to estimate feature length is from the projections through the thick section known as the ‘vertical section’. Feature length can be estimated by counting the number of intersections between the linear feature and isotropic planes in the projection of the 3D space. Gokhale [5] suggested a cycloid plane to represents the isotropic plane that intersects the linear feature. Figure 4.8 illustrates Gokhale’s method of estimating feature length using vertical section.

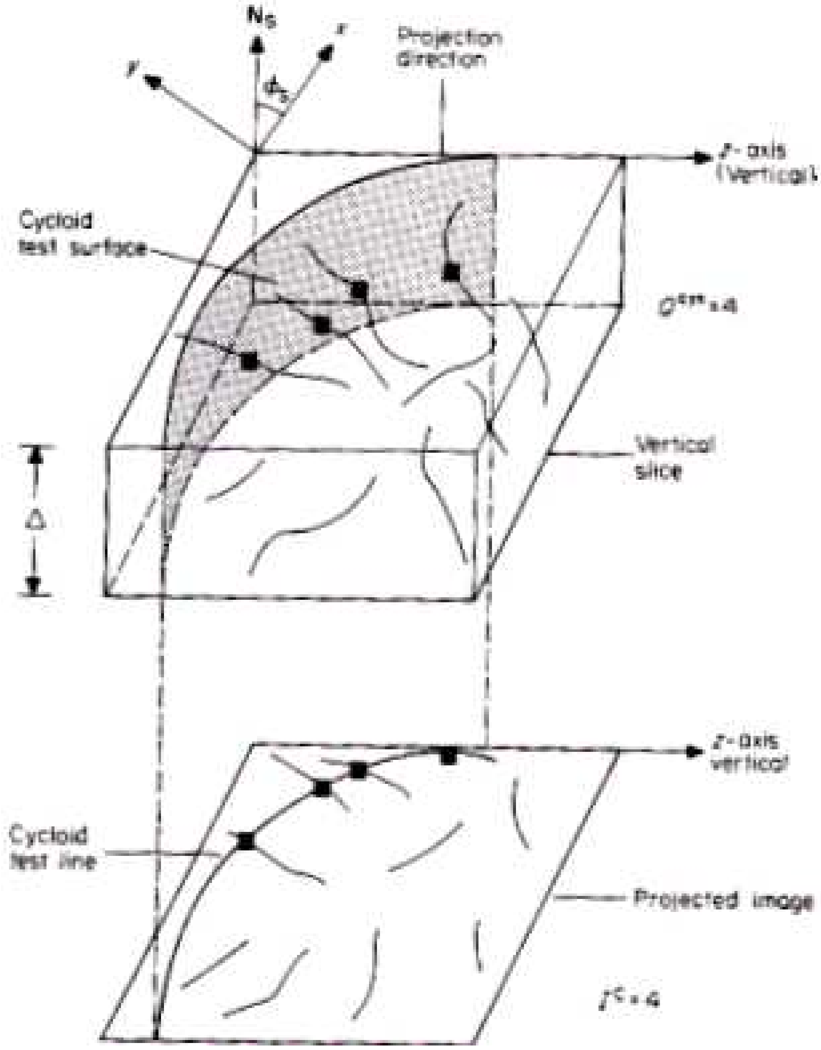

Figure 4.8: Estimation of feature length using vertical section and cycloid isotropic plane [5].

Hence the length density of linear features can be estimated from the following formula:

$$L_V = 2 \cdot \frac{I_{cl}}{T} \tag{4.8}$$

where L_V = length of feature per unit volume.
I_{cl} = number of intersections of cycloid test line with the projected images of linear feature of interest per unit test line length.
T = thickness.

Cruz-Orive and Howard [27] extended the concept of using cycloid plane to develop an unbiased estimator of the total length of bounded curves contained in an unbounded reference space (both thickness and volume $\rightarrow \infty$). To increase precision, a series of total vertical projections of the structure are obtained by starting with a random rotation about the vertical and then systematically rotating in a fixed angle.

Wulfsohn et al. [10] use the idea of 'total vertical projections' to estimate plant root lengths. They obtain the 'total vertical projections' by rotating the liner structure (plant root) about an arbitrary vertical axis, and projecting the linear structure onto a plane parallel to the axis of rotation. The total number of intersections between the cycloid arcs with their minor axis perpendicular to the axis of rotation and the projected linear structure than provides an unbiased estimator of the total length of the structure.

4.2 Projection

The geometry of projections involves problems that do not arise in sections cut through the opaque materials. Unlike stereology in sections, precise mathematical formulas and exact solutions in projection stereology are hardly available, and even in the simpler cases, approximate solutions may be the only ones available [1]. Projected images of microstructural features can be obtained from various sources, including thin sheets, film, or video capture.

4.2.1 Dimensionality

Before we proceed further, it is important to understand the dimensionality of an object in one dimension, two dimensions and three dimensions.

Table 4.1 describes dimensional equivalents for features in the plane projected to a line whereas Table 4.2 describes dimensional equivalents for features in 3D space projected to a plane.

Actual Dimensions	Projected Dimensions
0 (i.e. point)	0 (i.e. point)
1 (i.e. line)	0 (i.e. point) or 1 (i.e. line)
2 (i.e. area)	1 (i.e. line)

Table 4.1: Dimensional equivalents of spatial objects and their projected image for features in a plane projected to a line [1].

Actual Dimensions	Projected Dimensions
0 (i.e. point)	0 (i.e. point)
1 (i.e. line)	0 (i.e. point) or 1 (i.e. line)
2 (i.e. area)	1 (i.e. line) or 2 (i.e. area)
3 (i.e. volume)	2 (i.e. area)

Table 4.2: Dimensional equivalents of spatial objects and their projected images for features in space projected to a plane [1].

Table 4.1 implies that a zero dimensional feature such as a point on the plane will be projected as a zero dimensional feature too on the projection line, and one dimensional feature such as a line can either projected as a point (0D) or a line (1D). A two dimensional feature such as a circle on the plane will be projected as a one dimensional feature, a line. Table 4.2 implies similar dimensional equivalents for zero dimensional and one dimensional but different for two dimensional and three dimensional features. Instead of being projected as a one dimensional feature, a two dimensional feature in space can either be projected as a one or two dimensional feature on the projection plane. Lastly, three dimensional feature such as a sphere will be projected as a two dimensional circle (see Figure 4.9).

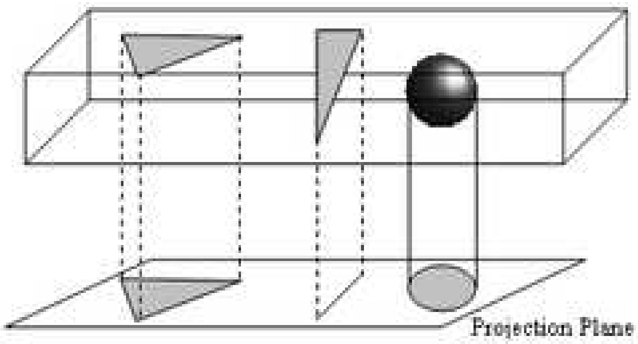

Figure 4.9: 2D and 3D features in space projected into a plane [1].

4.2.2 Points

As in section, points in projection are usually the resultant of intersections. It can be from intersection between a feature and test line or between surface area of feature and test point grid. Previously mentioned, projection of points is fairly straight forward and therefore the exact relationship can be expressed simply as:

$$P = P' \tag{4.9}$$

where P = number of actual intersection points.
P' = number of projected intersection points.

However, projected points create an ambiguity as they can be from actual points in space or a line perpendicular to the projection plane. Until now, there is no way to distinguish the sources of projection without supplementary information.

Suppose we have P_t intersection points between test points grid and surface area of feature in closed space with known thickness t, then the total test line length L_t is calculated by:

$$L_t = P_t \times t \tag{4.10}$$

Then the test area A_t is:

$$A_t = L_t \times t \tag{4.11}$$

Hence the test volume V_t is:

$$V_t = A_t \times t \tag{4.12}$$

From Equations (4.9), (4.10), (4.11), and (4.12), it is possible to derive formula for number of intersections per unit area P_A that is:

$$P_A = \frac{(P/L_t)}{t} \tag{4.13}$$

and the number of intersections per unit volume P_V that is:

$$P_V = \frac{(P/A_t)}{t} \tag{4.14}$$

4.2.3 Length of Lines

Lines in space can be projected either into points or lines, depending on the angle to the projection plane. Underwood [1] derived a mathematical relationship between the actual length of line and the apparent projected length of line by considering a straight line segment of length ℓ, with one end fixed and free to be rotated in any direction described by the angle ϕ (slant) and θ (tilt). Rotation of ℓ with both the angle ϕ and θ equal $\pi/2$ will generate one eighth of spherical surface of area $\frac{\pi \ell^2}{2}$ (see Figure 4.10).

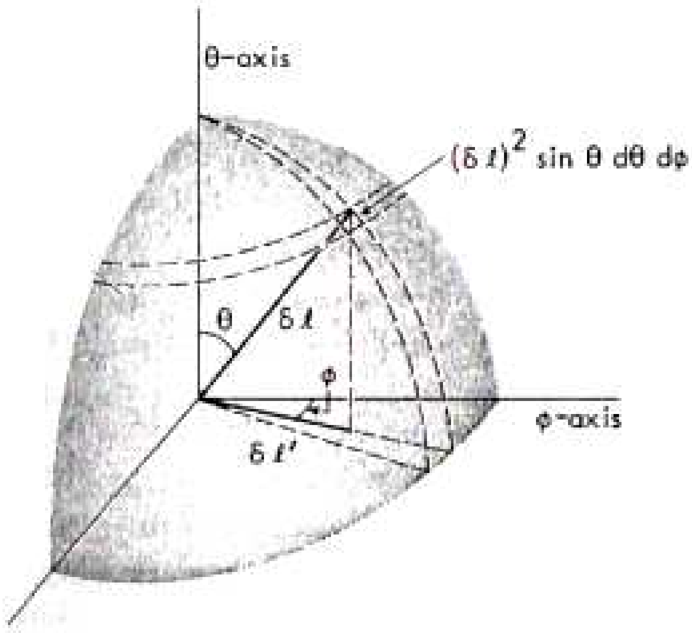

Figure 4.10: Average projected length of randomly oriented linear segment [1].

Thus, the average projected line length $\bar{\ell}$ is given by :

$$\bar{\ell} = \frac{\int_0^{\pi/2} \int_0^{\pi/2} \ell \sin\theta \, \ell^2 \sin\theta \, d\theta \, d\phi}{\pi \, \ell^2/2} \tag{4.15}$$

Since any curved line of length L can be represented by a sequence of straight line segments, then L is equal to the sum of ℓ ($\sum \ell$), hence we establish the relationship:

$$L = \frac{4}{\pi} L' \tag{4.16}$$

where L = actual length of line.
L' = apparent projected length of line.

4.2.4 Areas

Referring to Table 4.2, projected areas in a plane may arise from either surface of volumes in space or areas in space. Underwood [1] derived a relationship between surfaces of volume in space and its projected areas based on the derivation by Rudman [1]. The surface S of a particle is divided into elements ds, then the projected area dA' of each element on an arbitrary projection plane is given by:

$$dA' = n \cdot ds = ds(\cos\theta) \tag{4.17}$$

where n is unit normal and θ is the angle between the normal to the elements and the projection plane. Thus the average projected area $d\bar{A}'$ of an element ds taken over all orientations 4π is :

$$d\bar{A}' = \frac{ds}{4\pi}\int_0^{\pi/2} 2\pi\,\cos\theta\,\sin\theta\,d\theta\; = \frac{ds}{4} \tag{4.18}$$

where the integration limits $0 \rightarrow \pi/2$ extend only over the upper hemisphere. The lower hemisphere which is obscured between $\pi/2 \rightarrow \pi$ does not make contribution to the apparent projected area [1]. From Equation (4.18), the relationship between an object's surface area and its apparent projected area is given by:

$$S = 4\,A' \tag{4.19}$$

where S = actual surface area.
A' = apparent projeted area.

However Equation (4.19) is limited to a convex body. If the body is not convex (that is, if it contains reentrant surfaces), then it is possible for an element to be obscured even though $\theta < \pi/2$. Therefore, in general,

$$S \geq 4\,A' \tag{4.20}$$

where the equality holds in the limit of a convex body.

Equations (4.19),(4.20) relate the projected surface area of an object in space having the curvature of sphere to the actual surface area. For a randomly curved object, the projected area is given by:

$$S \geq 2\,A' \tag{4.21}$$

where the equality holds provided that loss of projected area by overlap or reentrant surfaces are negligible; otherwise the inequality becomes operative (total projection). Despite its limitation in handling particle overlap, Equation (4.21) is the only solution available for estimating the surface area of a random curvature particle.

4.2.5 Volume

Measurement of volume based on the projected image is a difficult task. To the extent of my research, there is no general solution available at present time. However Underwood [1] suggested a solution for estimating the volume of spherical particles with the assumption of no overlaps and surface re-entrants.

The volume, surface area, and mean projected area of a convex particle are related to the mean linear intercept $\bar{L_3}$. The original equation was stated in 1945 by Tomkeieff [28] and was later proved by Underwood [1] in 1970.

$$\bar{L_3} = 4\,\frac{V}{S} \tag{4.22}$$

where $\bar{L_3}$ = mean intercepted lengths from n random penetrations of
of a single particle by random straight test lines in 3D.
V = volume of a single particle.
S = surface area of a single particle.

Since $S = 4\,A'$ (Equation (4.19)), we obtain:

$$\bar{L_3} = \frac{V}{S} \tag{4.23}$$

Therefore the volume is given by:

$$V = \bar{L_3}\,A' \tag{4.24}$$

According to Underwood [1], $\bar{L_3}$ of a spherical particle is described by the following equation:

$$\bar{L_3} = \frac{2}{3}\,\overline{H'} \tag{4.25}$$

where $\overline{H'}$ is the mean tangent diameter and measured by taking the mean distance between parallel tangent planes for all orientations of a single particle. On an image, it is identical to the mean distance between parallel tangent lines for all orientations of a particle. Figure 4.11 illustrates the measurement of mean tangent diameter on the projection image.

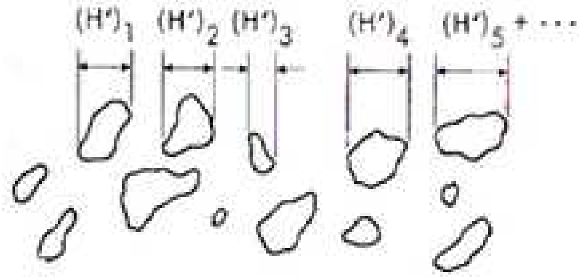

Figure 4.11: Measurement of mean tangent diameter on the projection plane [1].

Finally, based on Equations (4.24) and (4.25), Underwood expressed the volume of a spherical particle in the projection image as:

$$V = \frac{2}{3}\,\overline{H'}\,A' \tag{4.26}$$

where V = volume of a single particle.
$\overline{H'}$ = mean tangent diameter of a single particle.
A' = apparent projected area of a single particle.

However, Equation (4.26) is only valid for a spherical particle with the assumption that there is no surface overlap and truncation. In the case of a randomly curved particle, there is no solution available yet.

4.2.6 Volume Fraction

Volume fraction is a useful measurement to estimate the volume density of particles contained in a known volume space. Unlike with the section image, the volume fraction of a particle in a projection image is expressed in a more complicated way. Assuming there are finite numbers of spherical particles inside a box, the volume fraction of a spherical particle is derived through dividing both sides of Equation (4.26) by the volume of the box ($length \times width \times thickness$).

$$\frac{V}{V_{box}} = \frac{\frac{2}{3}\,A'\,\overline{H'}}{length_{box} \times width_{box} \times thicknessbox} \tag{4.27}$$

Since area of the box is $length_{box} \times width_{box}$, Equation (4.27) becomes :

$$\frac{V}{V_{box}} = \frac{\frac{2}{3}\,A'\,\overline{H'}}{area_{box} \times thicknessbox} \tag{4.28}$$

Consequently,

$$V_V = \frac{\frac{2}{3} A'_A \overline{H'}}{t} \tag{4.29}$$

where V_V = volume fraction of a spherical particle contained in a box.
A'_A = apparent projected area fraction of a spherical particle contained in a box.
$\overline{H'}$ = mean tangent diameter of a spherical particle contained in a box.
t = thickness of the box.

Again, Equation (4.29) is only valid for a spherical particle with the assumption that there is no surface overlap and no truncation.

4.3 Implementation

In this section I will describe the implementation of stereological methods based on projection stereology. The objective of this implementation is to estimate the geometrical properties of diatoms listed below :

- Number of diatoms.
- Average length of diatoms.
- Average surface area of diatoms.
- Average volume of diatoms.
- Volume fraction of diatoms.

All experiments discussed in this section are conducted based on a binary image of diatoms described previously in Chapter 3 (see Figure 3.7).

4.3.1 Number of Diatoms

Diatoms are represented by the white features in the binary image. In order to calculate the number of diatoms, each white feature is labelled based on four connectedness. The labelling operation is performed by using MATLAB function `bwlabel`. The last label number gives the number of white features (diatoms) in the image. The labelling process indicated that there are 66 diatoms in Figure 3.7. However, the calculation of diatoms quantity is only based on the observed diatoms in the image.

4.3.2 Length of Diatoms

There are two steps in estimating the length of a diatom from its projected image. First, the apparent length is measured and then the actual length is estimated using Equation (4.16). Measuring the apparent length of diatom is done by thinning the diatom and summing the distances between adjacent pixels. The thinning operation is done via the MATLAB function `bwmorph`. The function removes pixels so that an object without holes shrinks to a minimally connected stroke of pixels. There are two criteria in defining the distance between adjacent pixels; if they are straight, then the distance will be 1 (see Figure 4.12(a)) or if they are diagonal to each other, the distance will be $\sqrt{2}$ (see Figure 4.12(b)).

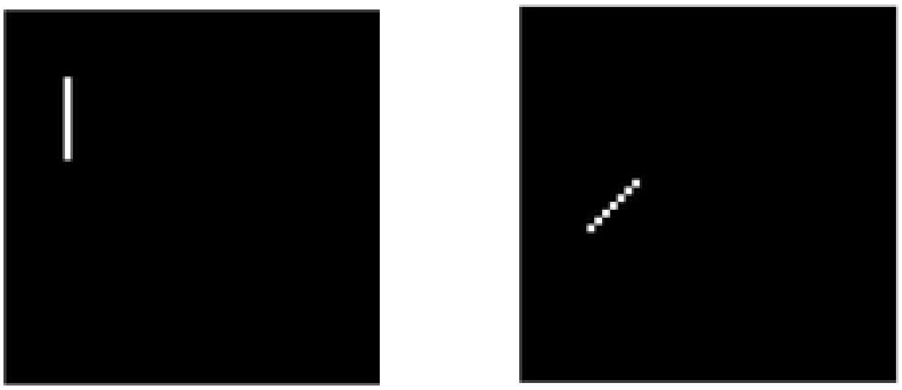

(a) Straight adjacent pixels.

(b) Diagonally adjacent pixels.

Figure 4.12: Two different orientation of neighbouring pixels.

However, if the diatom is only consisting of one pixel (there are no neighbouring pixels), the apparent length will be assumed to be 1. Once the apparent length of a diatom is calculated, its actual length is estimated using Equation (4.16). Suppose if a diatom's apparent length is 5 $pixels$, then the estimated actual length will be $5 \times \frac{4}{\pi} = 6.37$ $pixels$. A special procedure must be carried when measuring the apparent length of a diatom aggregate. Firstly, the branches must be separated out. Secondly, each individual branch length is calculated based on the two criteria mentioned before. Finally, the apparent length of a diatom aggregate is the sum of all individual branch apparent length. This procedure is justified because a diatom aggregate consisted of individual diatoms and its length will be the sum of all individual lengths. Figure 4.13 illustrates the process of dealing with a diatom aggregate.

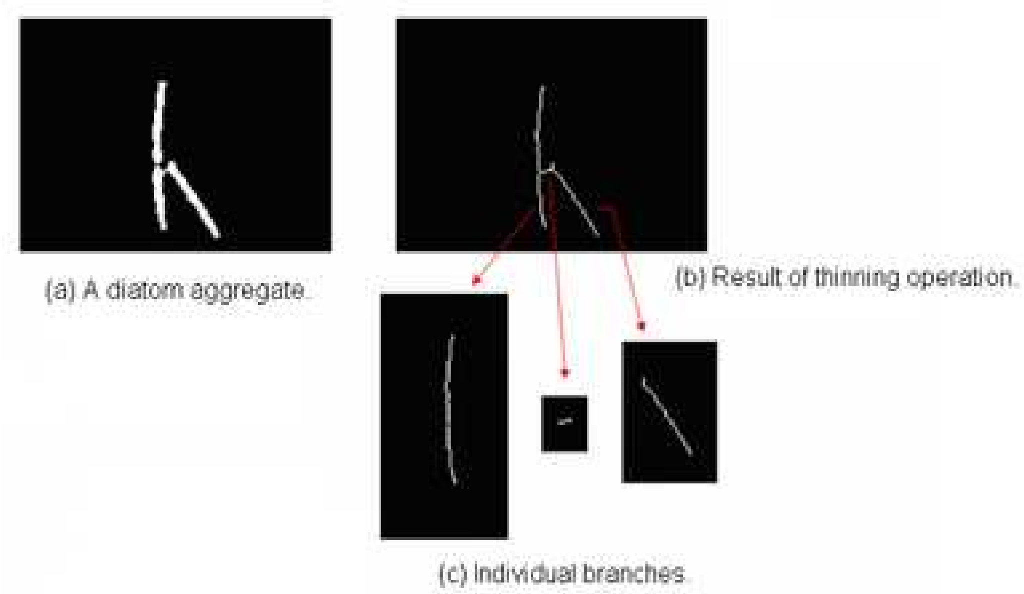

Figure 4.13: The process of measuring the apparent length of a diatom aggregate.

The estimation of actual length was carried out for all visible diatoms in the binary image. The experiment produced the average actual length of all diatoms as well as a table consisting of an apparent length and the corresponding actual length for all diatoms in the binary image (see Appendix B III). Figure 4.14 shows the binary image before estimation process and the binary image after estimation process.

(a) Binary image of diatoms before the estimation process.

(b) Binary image of diatoms after the estimation process.

Figure 4.14: The results of length estimation process.

4.3.3 Area of Diatoms

Similar to estimating the actual lengths of diatoms, there are two steps in estimating the surface area of a diatom. First, the apparent area from the projected image is calculated, and then the surface area of the diatom is estimated using Equation (4.19). To calculate the apparent area of a diatom, I have used MATLAB function `sum`, to sum all pixels that are on the white area. Hence the total number of pixels that are on the white area is an estimate of a diatom's apparent area. Since our diatoms are exhibiting random curvature, the surface area of a diatom is estimated using Equation (4.21).

Suppose a diatom's apparent area on the projected image is 10 $pixels^2$, then its surface area is 20 $pixels^2$ (2×10), with assumptions that there are no particles overlap and surface re-entrant. However if there are overlaps and re-entrants of surface, the surface area is estimated to be greater than 20 $pixels^2$.

The estimation of surface area was carried out on all visible diatoms in the binary image. The experiment produced the average surface area of all diatoms as well as a table consisting of apparent area and corresponding surface area for all diatoms in the binary image (see Appendix B IV).

4.3.4 Volume of Diatoms

As mentioned earlier, a volume estimation based on 2D projected image is a difficult task. Therefore, estimating an average volume of all diatoms gives more useful result than estimating an individual volume. Since there is no technique for estimating volume of randomly curved particles, the volume of diatoms are estimated based on the equation for spherical curvature.

To measure the average volume, Equation (4.26) is modified into:

$$\bar{V} = \frac{2}{3}\overline{\overline{H'}}\,\overline{A'} \tag{4.30}$$

where $\bar{V}$ = average volume of all diatoms.
$\overline{\overline{H'}}$ = average mean tangent diameter for all diatoms.
$\overline{A'}$ = average apparent projected area of all diatoms.

Firstly, the $\overline{\overline{H'}}$ value is obtained by averaging over individual diatom's mean tangent diameter. Since a diatom curvature is random, the mean tangent diameter is obtained by measuring the perpendicular distance between parallel tangent lines in any orientation. In this experiment, the vertical orientation was selected.

Therefore, the mean tangent diameter of a diatom is identical to perpendicular distance between parallel tangent lines in a vertical orientation. Figure 4.15 illustrates the measurement of mean tangent diameter.

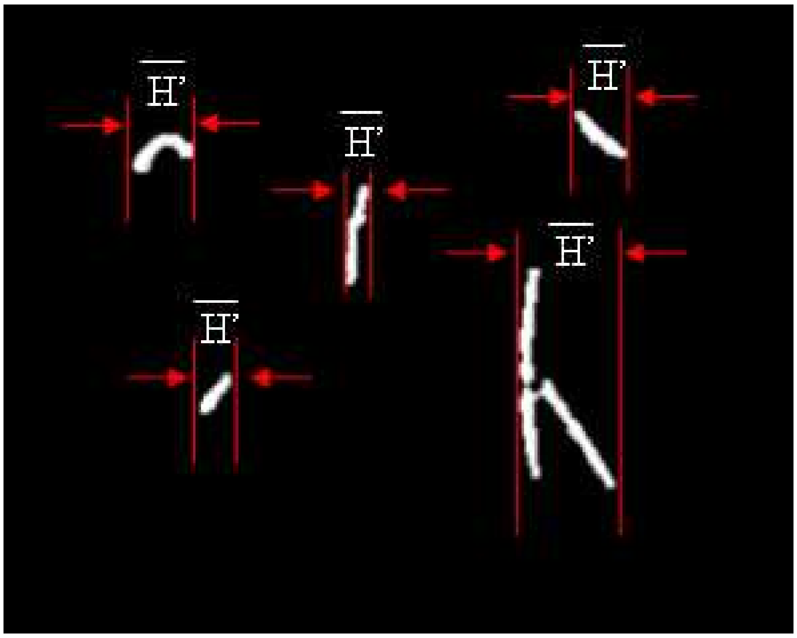

Figure 4.15: Mean tangent diameter of diatoms.

Subsequently, the $\overline{A'}$ value is obtained by taking an average of all diatoms' apparent area. Using the value of $\overline{\overline{H'}}$ and $\overline{A'}$, we can estimate the average volume of all diatoms from their projection image. An experiment was carried out to estimates diatoms' average volume and the results are presented in Appendix B V.

4.3.5 Volume Fraction of Diatoms

According to the Equation (4.29), the volume fraction of a spherical particle is related to its area fraction and mean tangent diameter. Although the curvature of a diatom is random, Equation (4.29) is still applied because it is the only technique available for estimating the volume fraction of a random curvature particle. Furthermore, the volume fraction of all diatoms (with respect to the volume of a bounding box) is a more useful quantity than the individual volume fraction; therefore, the Equation (4.29) is modified into:

$$V_{V\,total} = \frac{\frac{2}{3}\,A'_{A\,total}\,\overline{\overline{H'}}}{t} \tag{4.31}$$

where $V_{V\,total}$ = total volume fraction of all diatoms contained in a box.
$A'_{A\,total}$ = total apparent projected area fraction of all diatoms contained in a box.
$\overline{\overline{H'}}$ = average mean tangent diameter of all diatoms contained in a box.
t = thickness of the box.

The value of $A'_{A\,total}$ is calculated by:

$$A'_{A\,total} = \frac{A'_{total}}{image\ size} \tag{4.32}$$

where $A'_{A\,total}$ = total apparent projected area fraction of all diatoms contained in a box.
A'_{total} = total apparent projected area of all diatoms.
$image\ size$ = size of the image.

Assuming that the image of diatoms is an infinitely thin box, the thickness of the box t is identical to the camera depth of focus. An experiment was carried out to estimates diatoms' volume fraction and the results are presented in Appendix B VI. For the experiment, we assume that the depth of focus to be 5 $pixels$. In reality, the depth of focus depends on the camera setting.

CHAPTER 5

Validation of Stereological Results using Synthetic Diatom Simulator

All geometrical properties of diatoms deduced in Chapter 4 would be useless, unless there is a ground proof of the estimations obtained from the problem domain. Due to the time and budget constraint, experimenting with genuine diatoms to measure their geometries physically is impossible. However, I propose to generate a simulation of randomly structured synthetic diatoms that reflects the problem domain. This approach is acceptable since diatoms are randomly structured and oriented by nature.

The significance of simulating synthetic diatoms is to compare their actual geometries with geometries that are obtained through their 2D projection taken from a random view point. Based on the comparison, we can analyse the reliability of stereological methods in estimating geometrical properties of diatoms.

In the first section, I firstly describe the implementation of a synthetic diatoms simulator, followed by results from running the simulation. In the next section, comparisons between geometries of diatom obtained from the simulation and its 2D projection are presented and analysed. Finally, the last section presents discussion on the reliability of stereological methods in estimating diatoms' geometrical properties from their projection image.

5.1 Synthetic Diatom Simulator

The idea of synthetic diatom simulator is to generate randomly oriented and structured diatoms inside a bounding box with a given volume. The function that creates the simulator takes five parameters: *length of the bounding box, width of the bounding box, thickness of the bounding box, number of diatoms, and maximum length of diatoms.*

There are six main steps in generating a synthetic diatom simulator. Firstly, a bounding box is created based on the dimension specified by the user. Secondly, a diatom starting point in terms of x, y and z coordinate is defined randomly inside the bounding box using MATLAB function `rand`. Thirdly, to generate a randomly structured diatom, the length of a diatom is randomly defined between zero to a given maximum length. Furthermore, to generate a randomly oriented diatom, two orientation angles slant and tilt are defined randomly. Slant is a random value between 0 and π, while tilt is between 0 and 2π. Based on randomly generated length and orientation angles, the end point of a diatom can be calculated. In the fourth step, a synthetic diatom is constructed by filling in pixels between the starting point and the end point. Note that this synthetic diatom is only a line connecting between two points. A morphological dilation with circular structuring element is then applied to transform the line into valid representative of a real diatom. In addition, the algorithm repeats this process to generate the desired amount of diatoms.

Having created the 3D model of the synthetic diatoms, it is possible to obtain its 2D projection image along with several diatoms' geometries. A 3D model is represented by matrix with 3 dimensions (row, column and depth). Therefore, its 2D projection can be obtained by summing all the pixels along the third dimension (depth). This approach is considered unbiased since the synthetic diatoms are randomly structured and oriented. Figure 5.1 illustrates the results of simulating synthetic diatoms using various parameters (the corresponding 2D projection is shown next to the 3D model).

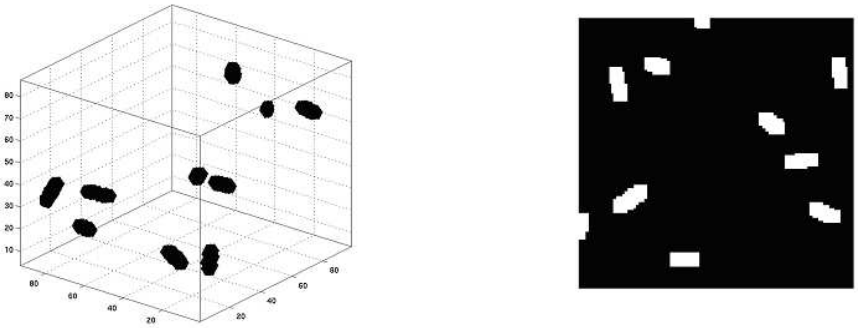

(a) Parameters used: bounding box dimension = 100 x 100 x 100 pixels^3, maximum length of synthetic diatom = 10 pixels and number of diatoms = 10.

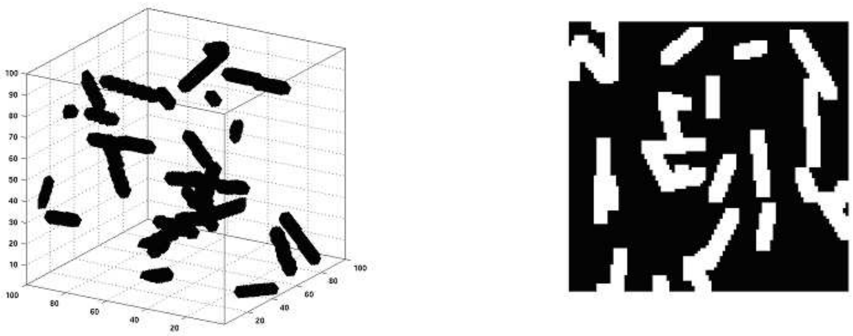

(b) Parameters used: bounding box dimension = 100 x 100 x 100 pixels^3, maximum length of synthetic diatom = 30 pixels and number of diatoms = 30.

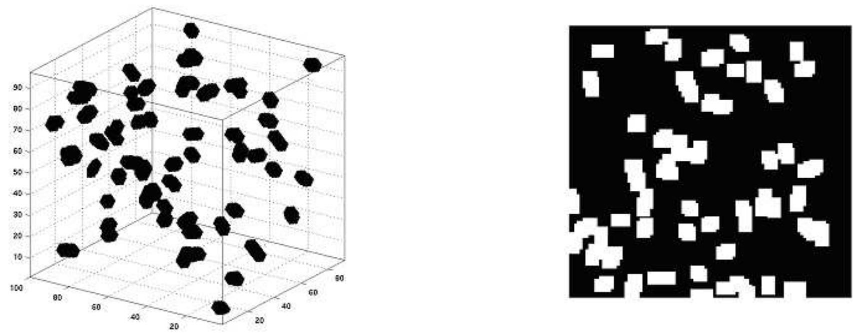

(c) Parameters used: bounding box dimension = 100 x 100 x 100 pixels^3, maximum length of synthetic diatom = 2 pixels and number of diatoms = 60.

Figure 5.1: The output of synthetic diatom simulator.

5.2 Comparison of Diatom Geometrical Properties

The synthetic diatom simulator is a useful tool to validate our estimation of diatoms' geometries from their projection image. The simulator produces two observations of diatom: a 3D model and the corresponding 2D projection image. Thus, enabling us to compare the result of stereological methods applied to the 2D projection image to its corresponding result obtained from the 3D model.

The experiment carried out in each subsection is independent to the experiment carried out in other subsection. All subsections are organised in the same way in that each subsection contains a methodology and followed by experimental results.

5.2.1 Number Comparison

Experimental Methodology

In order to create an unbiased comparison between numbers of diatoms observed in 2D image and how many are they actually exist in 3D, the input parameter *number of diatoms* should be modified into *maximum number of diatom*. Therefore, the number of iteration is determined by a random number between one to the *maximum number of diatom*.

I conducted two experiments with thirty simulations of synthetic diatoms for each experiment. In each simulation, the number of diatoms generated is random between one to the maximum number specified. Based on each of the corresponding projection image, a stereological method for estimating number of diatoms is applied. The first experiment was conducted with the following parameters:

- Volume space = $100 \times 100 \times 100\, pixels^3$.
- Maximum number of diatoms = 10.
- Maximum length of diatoms = $30\, pixels$.

Whereas the second experiment was conducted with the following parameters:

- Volume space = $300 \times 300 \times 300\, pixels^3$.
- Maximum number of diatoms = 60.
- Maximum length of diatoms = $30\, pixels$.

Experimental Results

The results of both experiments are shown in Appendix C I. The Table in the Appendix shows comparisons between the number of synthetic diatoms presents in the 3D model and the number of synthetic diatoms observed from the corresponding 2D projection. Additionally, a line chart is also presented to aids visual comparison. Based on the results, we conclude that the accuracy of the number estimation depends on the ratio between volume of the bounding box and the maximum number of diatom specified. One possibility that may cause an inaccuracy in the estimation is the chances of diatoms being overlapped by each other. As a result, two or more individual diatoms are projected into one if they are overlapping each other. However, when the ratio of bounding box volume to number of diatoms is large, the overlap frequency is decreasing, which makes an individual diatom projected merely without being overlapped by others.

5.2.2 Length Comparison

Experimental Methodology

The synthetic diatom simulator generates each synthetic diatom with a random length. Hence, each time a diatom is generated, its length is stored into the *actual length* buffer. I conducted an experiment with thirty simulations of synthetic diatoms. In each of the simulation, an average of synthetic diatoms' length is derived from the *actual length* buffer, then, compared to the average length estimated from the corresponding projected image via stereological method. In estimating the average length from the projected image, Equation (4.16) is used. However the length obtained from the projection image must be modified to take account the effect of dilation by a circular structuring element. For that reason, we must subtract the radius of the structuring element from the projection length in order to make a valid comparison to the original length. The experiment was conducted with the following parameters:

- Volume space $= 100 \times 100 \times 100\, pixels^3$.
- Number of diatoms $= 10$.
- Maximum length of diatoms $= 30\, pixels$.

The complete results of the experiment are presented in Appendix C II. The mean values of both averages shown in Table 5.1 indicate that the error in estimation is approximately 10% from the actual length. However, since a 2D projection image contains a limited information about the 3D space, an error of about 10% is the best that we can get.

	Average actual length (pixels)	Average estimated length from projection image (pixels)
Mean	14.8	13.3

Table 5.1: Mean of the average actual length and the average estimated length from projection image.

Deviation in the estimation process is mainly caused by an overlap between particles. When particles are overlapping, there are two possibilities, firstly, only parts of them are overlapped by others, and secondly, the whole body is overlapped by others. The first case is more significant by the second one, because when two or more synthetic diatoms are partially overlapped by each other, they are projected into one big diatom. Therefore in our estimation based on the projection image, we will have a projected length value which is larger than the average of two or more actual length values. Hence, it will lead us to an over estimation. Figure 5.2 illustrates a case where overlaps occurred. The real average length was 20.8 *pixels*, while the estimated average length was 29.7 *pixels*.

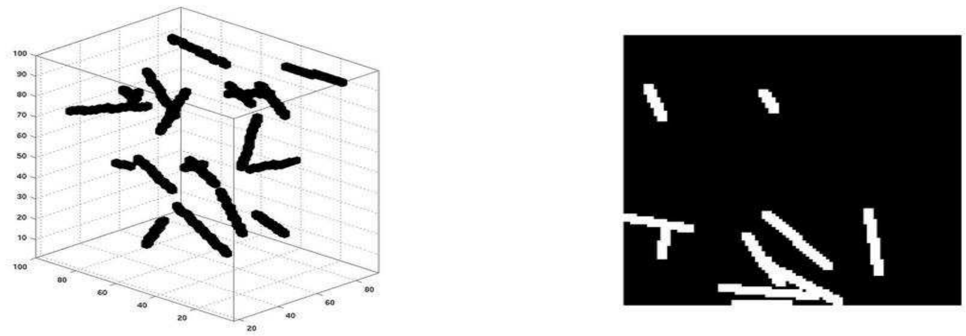

Figure 5.2: A 3D model of overlapping synthetic diatoms and its projected image.

However, it is also possible to have an under estimation and it is mainly caused by the orientation of the particle. Suppose if we have many particles that are perpendicular to the projection plane, only the top edge or the bottom edge of each particle are projected. Therefore, the average projected length will underestimate the actual average length.

5.2.3 Area Comparison

Experimental Methodology

Recall from Chapter 4, there are two formulas that describe the relationship between an object's actual surface area and its projected area. The first formula is for a spherical particle, while the second is for a random curvature particle. Therefore, I conducted two types of experiment; one is for spherical diatoms, and the other one is for random curvature diatoms.

For the first experiment, I ran thirty simulations of synthetic diatoms, where in each simulation, ten spherical diatoms are generated inside a $100 \times 100 \times 100$ bounding box. The length of each diatom is set to two pixels because we want them to closely approximate the shape of a sphere. Then, I calculated the surface area of each diatom and stored them into the *actual area* buffer. Since the volume of a spherical diatom can be calculated by summing all the pixels that made up that diatom, a theoretical surface area can be worked out. Given the volume of a sphere, the radius can be obtained through:

$$V = \frac{4}{3}\pi r^3 \tag{5.1}$$

where V = volume of the sphere.
r = radius of the sphere.

Having calculated the radius from the previous equation, the actual surface area of the sphere diatom is obtained by:

$$S = 4\pi r^2 \tag{5.2}$$

where S = surface area of the sphere diatom.
r = radius of the sphere.

The parameter setting for the second experiment is similar to the first experiment, except that each synthetic diatom generated is having a length of randomly between five to thirty pixels. Therefore, all diatoms generated will be randomly oriented and structured. The surface area of each diatom is calculated in the similar procedure as in the first experiment, except using the formula of a cylinder. This approach is compromised because a synthetic diatom that has a length of five pixels or more would appear as a thin cylinder (see Figure 5.3).

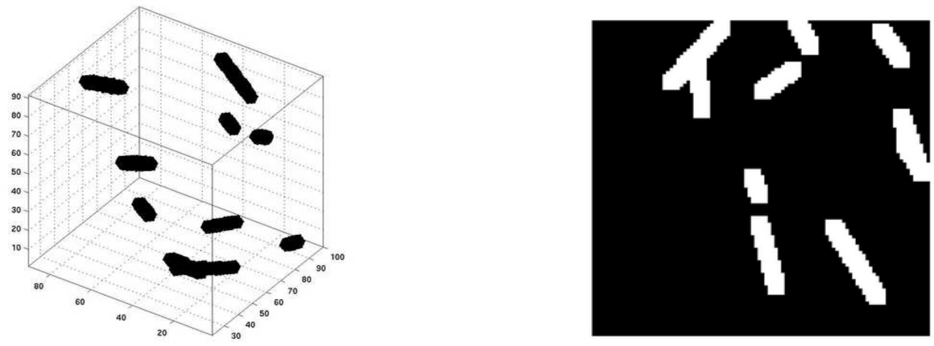

Figure 5.3: Diatom with length of five pixels or more appeared as a thin cylinder.

In each simulation of each experiment, an average of the surface area is derived from the *actual area* buffer and then compared to the average projected area obtained by applying a stereological method to the projection image. For the spherical diatoms, Equation (4.19) is used, whereas for random curvature diatoms, Equation 4.21 is used.

Experimental Results

The complete results for both experiments are presented in Appendix C III, whereas Table 5.2 presents the summary of the results.

	Experiment 1	Experiment 2
Mean of average actual surface area ($pixels^2$)	233.62	365.75
Mean of average estimated surface area from projection image ($pixels^2$)	241.17	249.18

Table 5.2: Mean of the average actual surface area and the average estimated surface area from projection image.

Surface Area - Experiment 1

The mean values presented in the Table 5.2 suggest that the error of estimation is approximately 3% from the actual surface area. The main contribution for this error has been the overlaps between particles. When a particle is fully overlapped by other in 3D space, it only appears as one particle size in the projected image (see Figure 5.4). Therefore, it will not affect the estimation process.

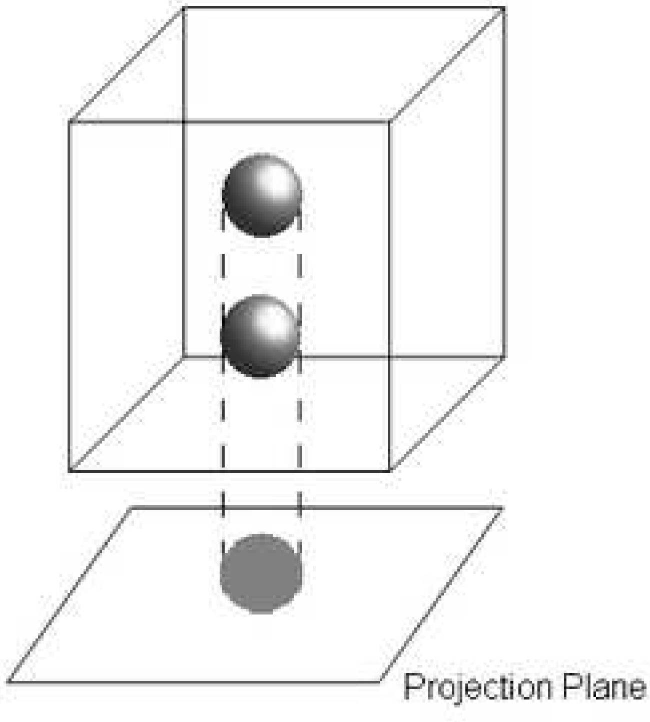

Figure 5.4: Projection of fully overlapped diatom.

But, when a particle is partially overlapped by other, it is projected as one particle with bigger area (see Figure 5.5). Hence, the estimation of the projected area will over estimate the actual surface area.

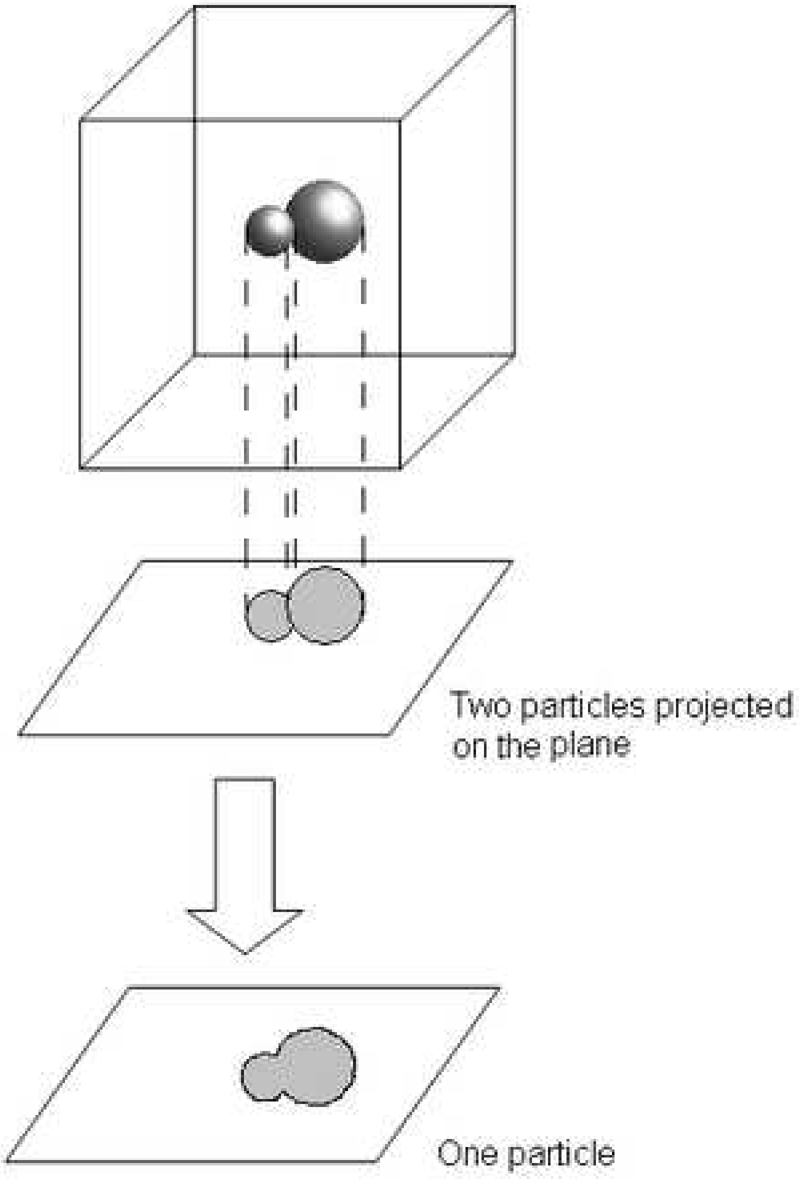

Figure 5.5: Projection of partially overlapped diatom.

Another cause of deviation is contributed through the truncation of particles by image frame. Particles that are on the edges of the bounding box are truncated in its projection image (see Figure 5.6). Consequently, the calculation of actual surface area is underestimated.

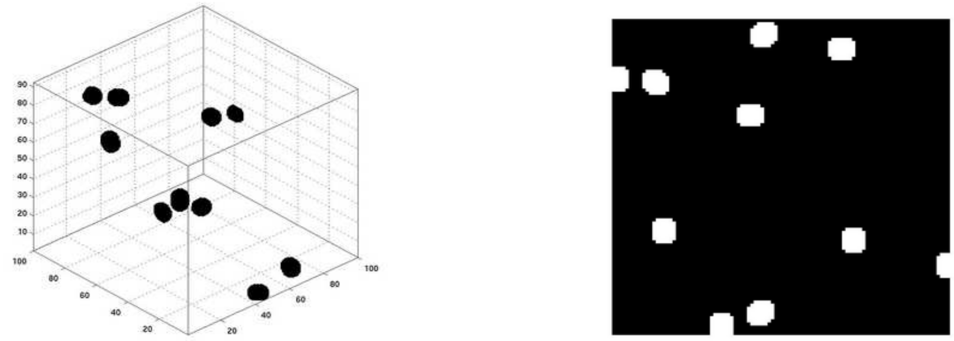

Figure 5.6: The red outlined diatoms in the projection image indicate that part of their area is truncated by the image frame.

Surface Area - Experiment 2

The mean values presented in the Table 5.2 suggest that there is a significant error of 22% from the actual average surface area calculation. However, our primary hypothesis for the second experiment is not the precision of the estimate, but whether or not, the experiment results satisfy the relationship depicted in Equation (4.21). According to Table 5.2 and the comparison chart in Figure 5.7, our hypothesis is satisfied, although there are some errors when the estimated average surface area from the projection is greater than the actual average surface area.

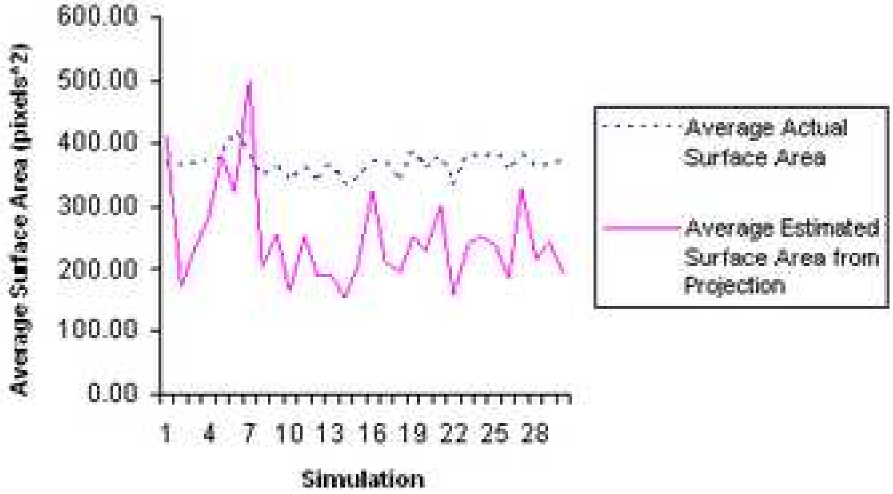

Figure 5.7: Comparison chart between the actual and estimated surface area of diatoms.

5.2.4 Volume Comparison

Experimental Methodology

As mentioned in Section 5.2.3, the actual volume of a synthetic diatom is calculated by summing all the pixels in the 3D matrix that made up the diatom. Therefore, each time a diatom is generated, its volume is calculated and then stored in the *actual volume* buffer.

Two experiments were conducted to compare the average volume of synthetic diatoms. The first experiment is for spherical diatoms, while the second is for random curvature diatoms. Other than the length, both experiments are using the same parameters listed below:

- Volume space = $100 \times 100 \times 100\, pixels^3$.
- Number of diatoms = 10.

In each experiment, thirty simulations were performed. In each simulation an average volume is derived from the *actual volume* buffer and then compared to the average volume estimated from the corresponding projected image. Since there is no available stereological method for estimating the volume of random curvature particles, both experiments used Equation (4.26) to estimate the average volume from the projection image. In this way we are approximating the random curvature with the spherical curvature.

Experimental Results

The complete results for both experiments are presented in Appendix C IV, whereas Table 5.3 presents the summary of the results.

	Experiment 1	Experiment 2
Mean of average actual volume ($pixels^3$)	309.97	175.67
Mean of average estimated volume from projection image ($pixels^3$)	271.19	314.82

Table 5.3: Mean of the average actual volume and the average estimated volume of diatoms from projection image.

Volume - Experiment 1

The mean values from both observations indicate that the error in the estimation is about 8% of the actual volume calculation. Since the volume estimation from projection image is related to the surface area estimation, the error can be seen as the consequence of the error in estimating the surface area.

Volume - Experiment 2

The mean values from both observations indicate that there is approximately 56% deviation from the average actual volume calculation. Despite the consequences of overlaps and truncations, the result of this experiment suggests that a spherical curvature is not at all appropriate for approximating the curvature of the diatoms, hence the volume. One of the factors that cause the deviation is the presence of elongated diatoms. The approximation of diatoms curvature based on spherical curvature will definitely deprived when many elongated diatoms are present.

5.2.5 Volume Fraction

Experimental Methodology

The volume fraction of all synthetic diatoms with respect to the volume of the bounding box is obtained by calculating the volume of all synthetic diatoms then divides it by the volume of the bounding box.

Two experiments were conducted to validate the estimation of the volume fraction of synthetic diatoms. The first experiment compares the volume fraction of spherical diatoms while the second compares the volume fraction of random curvature diatoms. Other than length, both experiments are using the same parameters listed below:

- Volume space = $100 \times 100 \times 100\, pixels^3$.
- Number of diatoms = 10.

In each of the experiment, thirty simulations were performed. In each simulation, the synthetic diatom's volume fraction is calculated and then compared to the volume fraction estimated from the corresponding projected image. Since there is no available stereological method for estimating the volume fraction of random curvature particles, both experiments used Equation (4.29) to estimate the volume fraction of diatoms from the projection image.

Experimental Results

The complete results for both experiments are presented in Appendix C V, whereas Table 5.4 presents the summary of the results.

	Experiment 1	Experiment 2
Actual volume fraction	13%	17%
Estimated volume fraction from projection image	10%	27%

Table 5.4: Mean of the actual volume fraction and the estimated volume fraction of diatoms from projection image.

Volume Fraction - Experiment 1

Table 5.4 summarises the result of the first experiment. The mean value from both observations indicates that the error in estimation of volume fraction from projection image is about 17% from the actual volume fraction calculation. The error in estimating volume fraction is highly dependant on the estimation of volume.

Volume Fraction - Experiment 2

The mean values from both observations indicate that there is about 37% deviation from the actual volume fraction calculation.

5.3 Summary

To conclude this chapter, a summary of all the estimations' accuracy are presented in Table 5.5.

Geometrical properties derived from projection image	Error from the actual properties for experiment 1 (%)	Error from the actual properties for experiment 2 (%)
1. Number of diatoms	9%	5.7%
2. Length of diatoms	10%	-
3. Surface area of diatoms	3%	22%
4. Volume of diatoms	8%	56%
5. Volume fraction	17%	37.2%

Table 5.5: Accuracy of the stereological estimation on all diatom geometrical properties.

Note that for estimation of diatom's length, I only conducted one type of experiment, because I assume that there is no difference between estimating the length of spherical particle and random curvature particle. Based on the figures shown in the table, estimating diatoms' area and volume from a projection image is a difficult task, and a reasonable estimation could not be made yet. But, when we assumed that diatoms are spherical in shape, we had a reasonably accurate estimation. In addition, it is likely that the percentage of error will be decreased when the size of the geometry increases.

CHAPTER 6

Conclusions and Further Study

In 1997 Waite et al. [7] developed videography, which is a method of sampling diatoms that minimises the interruption of diatoms structure during the process. However, the quality of the sample image is poor, which makes in-depth analysis of diatoms in the image difficult.

The primary focus of the work in this project is on the enhancement of diatom images and the subsequent use of stereology to deduce geometrical properties of diatoms. Firstly, I have implemented a series of techniques for diatom image enhancement to facilitate the estimation of diatoms' geometrical properties. Experiments were then conducted using a diatom image supplied by The Centre of Water Research of UWA. The experimental results have shown that a combination of image processing techniques is able to effectively enhance the clarity of the diatoms while reducing the noise. However the enhancement process is highly dependant on the parameters used such as the denoising parameters, the size of the structuring element and the thresholding values. Overall, the results have shown that processing the diatom images is an essential stage prior to the application of stereology to deduce geometrical properties of diatom.

Since the image of diatoms sampled through videography represents a projection of diatoms, I have implemented stereological methods based on the projection image to deduce geometrical properties of diatoms. An experiment was conducted using the processed image to estimate the following properties:

- Number of diatoms.
- Length of diatoms.
- Surface area of diatoms.
- Volume of diatoms.
- Volume fraction of diatoms.

The experimental results were then presented as an average estimation of each of the properties listed above. However, we are unable to validate the results of the experiments because obtaining a physical measurement of diatoms' geometries is impossible in practice.

To resolve the difficulty in validating the results of stereological method, I have implemented a synthetic diatom simulator. The simulator produces the 3D model of diatoms as well as the corresponding projection image. The 3D model contains randomly generated diatoms with random orientations, whereas the 2D projection image was taken by projecting the 3D model along the depth axis. The simulator has enabled us to obtain the true measurement of diatoms' geometrical properties. Experiments were conducted by applying stereological methods on the projection image to estimate geometrical properties of diatoms. Then, the results were validated against the measurement obtained from the corresponding 3D model of the projection image. For experiments with spherical diatoms, the validations have shown reasonably accurate results despite the occurrences of overlaps and truncations between the particles. However, in the case of random curvature diatoms, the percentage error from the actual geometries measurement is still at significant level. Apart from of overlaps and truncation, the large deviation in random curvature case has proved that currently available stereological methods are inadequate to provide a decent approximation of diatoms' geometries.

Overall, I have implemented a set of techniques for analysing a diatom image. Although these techniques are still premature in terms of their accuracy, they can serve as the basis of further study of diatoms geometries. In addition, the stereological methods implemented can be tuned to suit the curvature of other object, if one desires to study the geometries of the object based on its projection image.

Further research that can be carried out include the following:

- A research on metric to evaluate the fidelity of the binary image.
- The experimental results have shown that the main factors contributing to the error in estimation are overlaps between particles and truncation of particles by the field of view. An investigation of how to deal with them may help to reduce the error in estimation process. Such investigation should start on how to identify whether overlaps and truncations occur, followed by ways of handling them when they occur.
- To increase accuracy of the stereological estimations, one can average the estimation from several different observations of diatom. However, this

requires taking images of diatom in the same view plane but different orientations. Thus, in the diatom simulation, we can mimic this process by taking projections of diatom from more than one viewpoint and obtain better estimation.

- A development of stereological relationship between the real object and its projection for different variety of curvatures. Therefore, when working with random curvature objects, we can have a better approximation of curvature. For example, a better curvature approximation of an elongated diatom will be a thin cylinder curvature or a thin ellipse, rather than the spherical ones.

- Further statistical study to validate the estimation should be conducted. For example, a confidence interval evaluation should be carried out to support the correctness of the estimation. Moreover, experimenting with a large datasets will always give a credible outcome.

APPENDIX A

Original Honours Proposal

This is meant to be a blank page, replace with something...
This is meant to be a blank page, replace with something...

This is meant to be a blank page, replace with something...

This is meant to be a blank page, replace with something..

This is meant to be a blank page, replace with something...

APPENDIX B

Experimental Results of Chapter 4

This is meant to be a blank page, replace with something...
This is meant to be a blank page, replace with something...

This is meant to be a blank page, replace with something...

This is meant to be a blank page, replace with something...

This is meant to be a blank page, replace with something..

APPENDIX C

Experimental Results of Chapter 5

This is meant to be a blank page, replace with something..
This is meant to be a blank page, replace with something..

This is meant to be a blank page, replace with something...

This is meant to be a blank page, replace with something...

This is meant to be a blank page, replace with something...

This is meant to be a blank page, replace with something...

This is meant to be a blank page, replace with something...

This is meant to be a blank page, replace with something...

This is meant to be a blank page, replace with something...

This is meant to be a blank page, replace with something..

This is meant to be a blank page, replace with something...

Bibliography

[1] Ervin E. Underwood. *Quantitative Stereology.* Addison Wesley Pub. Co., 1970.

[2] P. D. Kovesi. Phase preserving denoising of images. In *The Australian Pattern Recognition Society, Conference on Digital Image Computing: Techniques and Applications*, pages 68–73, December 1999. Perth.

[3] C.V. Howard and M.G. Howard. *Unbiased Stereology.* BIOS Scientific Publishers, 9 Newtec Place, Magdalen Road, Oxford OX4 IRE, UK, 1998.

[4] H.J.G. Gundersen. Notes on the estimation of the numerical density of arbitrary profiles: the edge effect. *J. Microsc.*, 111:219–223, 1977.

[5] A.M. Gokhale. Unbiased estimation of curve length in 3-D using vertical slices. *J. Microsc.*, 159:133–141, August 1990.

[6] C. Field, M. Behrenfeld, J. Randerson, and P. Falkowsky. Primary production of the biosphere: integrating terrestial and oceanic components. *Science*, 281:237–240, 1998.

[7] Anya Waite, Scott Gallager, and Hans G. Dam. New measurements of phytoplankton aggregation in a flocculator using videography and image analysis. *Marine Ecology Progress Series*, 155:77–88, 1997.

[8] A.J. Baddeley. Stereology and survey sampling theory. In *Bull. Intern. Statis. Inst., Proceedings 49th Session*, pages 50 (2): 435–449. Florence, 1993.

[9] Vojilav V.Mitic, Zoran S. Nikolic, Ivona Mitrovic, Branka Jordovic, and Vladimir Brankov. The application of stereology method for estimating the number of 3D BaTiO3 - ceramic grains contact surfaces. *Image Analysis and Stereology*, 20:231 – 237, 2001.

[10] Dvorlai Wulfsohn, Jens R. Nyengaard, Hans Jorgen G. Gundersen, Adrian J. Cutler, and Timothy M. Squires. Non-destructive, stereological estimation of plant root lengths, branching pattern and diameter distribution. *Plant and Soil*, 214:15–26, 1999.

[11] Jacob R. Glaser and Edmund M. Glaser. Stereology, morphometry, and mapping: the whole is greater than the sum of its part. *Journal of Chemical Neuroanatomy.*, 20:115–126, 2000.

[12] T. Kiorboe, K. P. Andersen, and H. G. Dam. Coangulation efficiency and aggregate formation in marine phytoplankton. *Marine Biology*, 107:235–245, 1990. Cited in Waite et al., New measurement of phytoplankton aggregation in a flocculator using videography and image analysis. Marine Ecology Progress Series 1997, 155:77-88.

[13] M.G. Forero-Vargas, R. Redondo, and G. Cristobal. Diatom screening and analysis by shape from contour. In *International Workshop VLBV*03, Visual Content Processing and Representation*, Madrid, 2003. Instituo de Optica (CSIC).

[14] Michael H. F. Wilkinson, Jos B. T. M. Roerdink, Stephen Droop, and Micha Bayer. Diatom contour analysis using morphological curvature scale spaces. In *Proc. 15th Intern. Conf. on Pattern Recognition (ICPR'2000)*, pages 656–659, Barcelona, Sep. 3-7 2000.

[15] H.Shahbazkia, T.Candeias, R.Oliveira, and F.Tomaz. Weighted morphometric shape analysis of diatoms. *RECPAD*, 2002.

[16] N. Otsu. A threshold selection method from gray level histograms. *IEEE Trans. Systems, Man and Cybernetics*, 9:62–66, March 1979. minimize inter class variance.

[17] Jan Flusser and Tomas Suk. Affine moment invariants: A new tool for character recognition. *Pattern Recognition Letters*, 15:433–436, 1994.

[18] Alan V. Oppenheim and Jae S. Lim. The importance of phase in signals. In *Proceedings of the IEEE 69*, pages 529–541, 1981.

[19] J. Canny. A computational approach to edge detection. *IEEE Transactions on Pattern Analysis and Machine Intelligence*, 8(6):679–698, November 1986.

[20] N. Roberts, L. M. Cruz-Orive, N. Reid, D. Brodie, M. Bourne, and R. H. T. Edwards. Unbiased estimation of whole body composition in humans by cavalieri's method using magnetic resonance imaging. *J. Microsc.*, 171:239–255, 1993.

[21] Benyamin Sahin, Heseyin Aslan, Bunyami Unal, Sinan Canan, Sait Bilgic, Suleyman Kaplan, and Levent Tumkaya. Brain volumes of the lamb, rat

and bird do not show hemispheric assymetry: a stereological study. *Image Analysis and Stereology*, 20:9–13, 2001.

[22] E. Thompson. Quantitive microscopic analysis. *J. Geol.*, 38:193, 1930.

[23] E. Artacho-Perula and R. Roldan Villalobos. Unbiased stereological estimationof the number and volume of nuclei and nuclear size variability in invasive ductal breast carcinomas. *J. Microsc.*, 186:133–142, May 1997.

[24] Terry M. Mayhew. Fibrin-type fibrinoid in human placenta: a stereological analysis of its association with intervillous volume and villous surface area. *Image Analysis and Stereology*, 20:1–7, 2001.

[25] D.C. Sterio. The unbiased estimation of number and sizes of arbitrary particles using the disector. *J. Microsc.*, 134:127–136, 1984.

[26] Zoltan Tomori, Ivan Krekule, and Lucie Kubinova. Disector program for unbiased estimation of particle number, numerical density and mean volume. *Image Analysis Streology*, 20:119–130, June 2001.

[27] L.M. Cruz-Orive and C.V. Howard. Estimating the length of a bounded curve in three dimensions using total vertical projections. *J. Microsc.*, 163:101–113, 1991.

[28] C.S. Smith and L. Guttman. Measurement of internal boundaries in three-dimensional structures by random sectioning. *Trans. AIME*, 197:81, 1953.